GOLD NANOPARTICLE-BASED LATERAL FLOW KIT FOR *IN VITRO* DETECTION OF MALARIA ANTIBODIES

By

CHRISTIAN LUNGANI MTHEMBU

Student Number: 21011968

Submitted in fulfilment of the requirements of the Master of Applied Science in Chemistry in the Faculty of Applied Sciences at the Durban University of Technology

July 2018

DECLARATION

I hereby declare this work forming a Dissertation, which I with its content submit for the qualification

MASTER OF APPLIED SCIENCES IN CHEMISTRY

To the Chemistry Department in the Durban University of Technology, further declare with assistance of the mentioned supervisor(s) it as my own work which has never been submitted to any University by me or anyone for a qualification.

on this 19th day of July 2018

Mr. C.L Mthembu *(Student)*

on this 19th day of July 2018

Dr P.S Mdluli *(Supervisor)*

on this 19th day of July 2018

Dr M. Mlambo *(Co-supervisor)*

on this 19th day of July 2018

Mr H. Gumede *(Co-supervisor)*

AKNOWLEDGEMENTS

I would like to express my sincere gratitude to the following people my supervisor Dr Phumlani Selby Mdluli, co – supervisors Dr Mbuso Mlambo and Mr Halalisani Gumede for their assistance throughout this endeavour.

A special thanks to Dr Myalowenkosi Innocent Sabela for all he has taught me about research experiments, writing and providing all the support I needed through the most tribulations without which I would not be at this stage. Thank you for inspiring in me the courage to embark on this journey and being there every step till the end.

I would also like to thank the National Research Foundation, Eskom and Mintek for financial support. Without their assistance, this would not be possible.

Thank you to the Technology Innovation Agency (Bioprocessing platform) for supporting me technically, financially and allowing me time to embark on this journey, I truly appreciate.

DEDICATION

This work is dedicated to my family and friends. Special dedication to all those who couldn’t finish their master’s qualification, it is possible.

This is dedicated to my father Mr Joseph Hlanganani Mthembu, thank you for making sure that I get the best you could offer and for all the support throughout my studies. And thank my mother, Maria Ncameleni Mthembu for always being there to support me. I would also convey my sincere gratitude to god, without his will, this would not be realized.

Thank you to my late grandfather, Dibhuloni Stephan Mthembu, who inspired in me the love for education at a young age.

ABSTRACT

This study involves the development of three-dimensional dual lateral flow diagnostic assays. These assays were fabricated with quick response (QR) barcodes to ease the accessibility and transfer test data. The assays were designed to also improve the collection and transfer of survey from point-of-care facilities to centralized laboratories, thus, these would help to speed-up response to disease out-break. The study introduces the fabrication of two barcode based malaria diagnostic in the field of diagnostics. Two lateral flow kits were modified with two QR barcodes and three QR barcodes encoded with Google analytics codes for the detection and real-time tracking of malaria lateral flow which was designed to detect *Plasmodium lactate dehydrogenase* (pLDH). The fabrication of test kit was achieved by attaching two and three QR barcodes into two different test kits which were encoded with websites that were linked to Google analytics website as a tracking and performance monitor. Gold nanoparticles (AuNPs) were used as a substrate, where optical and structural properties were studied using UV/Visible spectroscopy, fluorescence spectroscopy, and transmission electron microscopy (TEM).

The anti-mouse IgG antibody was used as a secondary antibody to act as control and the anti-(pLDH) was stripped on the test line. Phosphate buffer was used as a mobile phase solution. The antibody binding with pLDH antigen showed red test line indicating a positive test. Two diagnostic kits for rapid detection of pLDH were developed and validated for the detection of malaria antigen with lowest detectable recombinant concentration of 10 $ng.mL^{-1}$. The diagnostic kits were incorporated with two and three optimally angled QR barcodes for identifying positive and negative. The second three QR barcode embedded test kit identified positive, negative and invalid using tracked website. These QR barcodes enabled massive results and tracking with precise location of the test through Google Analytics.

Table of Contents

List of Figures

List of Tables

List of Abbreviations

AuNPs	: Gold nanoparticles
DNA	: Deoxyribose Nucleic Acid
HIV	: Human Immunodeficiency Virus
IgG	: Immunoglobulin
HcG	: Human Chorionic Gonadotrophin
PCR	: Polymerase Chain Reaction
qPCR	: Quantitative Polymerase Chain Reaction
CTEM	: Conventional Transmission Electron Microscopy
PFHRP2	: Plasmodium Falciparum Histidine Rich Protein – 2
pLDH	: Plasmodium Lactate Dehydrogenase
SEM	: Scanning Electron Microscopy
NR	: Not Reported
QR	: Quick Response
GA	: Google Analytics
AGP	: Glycoprotein
HGPRT	: hypoxanthine – guanine phosphorybosyltranserase
CBZ	: Cabozantib
TFB	: Tofacitinib
RGB	: Red Green Blue
HTML	: HyperText Markup Language
HAS	: Hue Saturation Value
RGB	: Red Green Blue
ELISA	: Enzyme-linked immunosorbent assay
AuNC	: Gold nanocluster

ANNEXURE

Research Outputs

Oral Presentations

The Technology Innovation Agency WELCOMES The **Parliamentary Portfolio Committee on Science & Technology** to TIA's Structures, Programmes & Projects in KZN 29 March **2017**. "*Quick Response Lateral Flow Assay*"

Durban University of Technology, staff aiming higher. **Faculty of applied sciences research day**, 11 December **2017**. "*Google Analytics and quick response dual lateral flow immunoassay for malaria"*

Durban University of Technology, **Chrom SA, SACI**, 02 February **2018**, "A Quick response and Google Analytics advancement of gold nanoparticle-based dual lateral flow immunoassay for malaria – (pLDH)"

University of Nairobi, International Inorganic Chemistry Conference, Best Western Maridian Hotel – **Kenya**, 23 May **2018**, *"A Quick response and Google Analytics advancement of gold nanoparticle-based dual lateral flow immunoassay for malaria"*

Poster Presentations

EThekwini Municipality and the Human Sciences Research Council (HSRC) invites you to the 5th the **Annual Research Symposium**. Strengthening Research Collaboration to Support Radical City Transformation, 01 June **2017**. "*A Google Analytics Tracked; Quick Response Code Based Lateral Flow Immunoassay For Onsite Detection of Malaria".*

Manuscripts Published

Christian L. Mthembu, Myalowenkosi I. Sabela, Mbuso Mlambo, Lawrence M. Madikizela, Suvardhan Kanchi, Halalisani Gumede, and Phumlane S. Mdluli "Google Analytics and quick response for advancement of gold nanoparticle-

based dual lateral flow immunoassay for malaria – *Plasmodium* lactate dehydrogenase (pLDH)", Analytical Methods, 9 (2017): 5923-5982

Manuscripts in Preparation

Christian L. Mthembu, Myalowenkosi I. Sabela and Phumlane S. Mdluli, "Trends in lateral flow applications for infectious disease detection – Review"

CHAPTER 1

Introduction

1. Introduction

Malaria is a serious challenge in Africa and mostly sub-Saharan countries. Until today, travellers from South Africa and other countries are still required to verify malaria infection before they can be allowed entry into some countries. It is one of the diseases contributing to most mortality in tropical countries especially in Africa. Over one million children die from malaria annually and it affects more than 500 million people worldwide (Azikiwe *et al.* 2012). It remains a global health problem to humans in tropical and subtropical countries as a leading cause of death leaving 3,3 billion people in 97 countries at risk (Cowman *et al.* 2016), and around 600 000 deaths (Cowman *et al.* 2016). Until the 19th century, malaria was endemic in most countries in the world, carrying the capability of distracting a country's economy (Abraham, Massebo and Lindtjørn 2017). Country like Ethiopia, malaria is a huge public health problem affecting more than 65% of the population occupying 75% of the high risk of infection classified land mass (Endeshaw *et al.* 2010). Malaria is a parasitic disease obtained from an infected mosquito bite, and in humans, it is caused by six species of *Plasmodium*, *vivax*; *ovale curtisi*; *ovale wallikeri*; *malariae* and *falciparum*, *lactate dehydrogenase* (pLDH), and the latter is usually considered the most contributer of deaths (Cowman *et al.* 2016). Malaria infection and lifecycle was elaborated by Alan F. Cowman. Briefly, the infection is initiated through the injection of sporozoites (spzs) into the dermis by a feeding female anopheline mosquito, spzs enter the vasculature and transported into the liver where they exit the sinosoids through the kupffer or endothelial cells and enter a hepatocyte. Active invasion preceded by cellular traversal until a suitable hepatocyte is found resulting to formation of parasitophorous vacuole membrane (PVM) which undergoes schizogony until tens of thousands of daughter merozoites are released in packets of merosomes into the vasculature (Hansen *et al.* 2014; Cowman *et al.* 2016). There, they then encounter erythrocytes and begin a chronic cycle of asexual schizogony in bloodstream. A proportion of asexually reproducing merozoites are reprogrammed to undergo gametocytogenesis, where within 15 days, gametocytes sequester develop within the bone marrow, and once mature, enter the peripheral circulation for

ingestion by a mosquito where they merge as extracellular male and female gametes in the midgut. Mating occurs by fusion of micro- and macrogametes to form a zygote transforming over 24 hours into a ookinete that migrates through the mosquito midgut epithelium and encysts to become an oocyst where asexual sporogenic replication occurs. Motile sporozoites are then released into the hemocoel by oocyst rupture and pass into salivary glands where they can be injected into the next human host (Cowman *et al.* 2016). Other types of malaria parasites and infections can be the biggest threats to human life e.g. cerebral malaria, an infection of the cerebral distracting neurological makeup in the human host, this type of malaria infection has taken lives of African children within 1 – 2 days of admission to hospital (Moussa *et al.* 2017).

Symptoms of malaria are tricky to conclude, manifesting in different ways to different patients infected such as muscle pains, headache, nausea and rigors (Cowman *et al.* 2016). Limited number of tools for malaria prevention and the inability to completely eradicate the disease have led to development of vaccines, as vaccines have been the only foreseeable type of immunoprophylaxis against malaria (Rodrigues and Soares 2014).

Over the past 15 years, endemic countries have observed a decline in malaria prevalence since the control and elimination efforts rejuvenated through the eradication agenda for malaria (Auburn and Barry 2017). Density, sporozoite rate and entomological inoculation rate (EIR) were parameters utilized for assessing the intensity of malaria transmission and impact of interventions through the principal strategy to reduce the burden of malaria in Ethiopia (Abraham, Massebo and Lindtjørn 2017). Thus, there is a dire need of the early diagnosis of malaria remains the only imminent solution which could be utilized to get rid of the scourge, and early infections. Lateral flow assays as a tool of early screening and diagnosis of malaria have gained much attention of researchers due to their low cost, user friendly formats, little interferences, short assay times and easily operated by un-skilled personnel (Bahadır and Sezgintürk 2016). They have been extensively used for point-of-care (POC) self-diagnostics with advantage of being a user friendly and however they have

a drawback due to their application to quantify the extent of infection (Fu *et al.* 2016), it is therefore not amazing that there is always a need for reference laboratory where positive malaria test has been found so that more informed conclusions can be made. Lateral flow devices provide a prompt detection, for simply yes or no decision and easy usage, also don't require complex analytical knowledge or equipment and enable on-site detection (Fischer *et al.* 2017). A simple urine based pregnancy test for home use were first launched commercially in 1984, offering results through a colour change signal visible to the eye and easy to interpret (Mak, Beni and Turner 2016). They are often referred to as rapid diagnostic tests (RDTs) offering fast diagnosis and reliability (Hathiwala *et al.* 2017). Lateral flow devices provide a prompt detection (Fischer *et al.* 2017), are accurate and rapid (Ang *et al.* 2016), offers simplicity of readout (Mak, Beni and Turner 2016), high specificity and sensitivity dependent on parasite level (Oyeyemi *et al.* 2016).

Malaria has been studied through a lot of different techniques and analysed, according to Sarah Auburn and Alyssa E. Barry, molecular approaches have been used extensively for surveillance of malaria populations (Auburn and Barry 2017). While quantitative polymerase chain reaction qPCR was observed to be the most sensitive and specific method compare to microscopy (Dakić *et al.* 2014). Endeshaw and co-workers compared the methods of malaria detection Parascreen and Paracheck vs microscopy and found Parascreen to be more useful where microscopy is unavailable (Endeshaw *et al.* 2010). Current methods to detect malaria are listed in Table 1.1 below:

Table 1.1: Techniques used to detect Malaria in blood samples and their disadvantages

Method	Technique	Limitation
Molecular Methods	Molecular level technique	Laboratory & skilled personnel
PCR	DNA technique	Laboratory & skilled personnel
Lateral flow	Rapid test kit	Sensitivity
LED florescence Microscopy	Magnification technique	Requires skilled personnel and high maintenance
Piezoelectric immunosensor	Electro-Analytical	Requires skilled personnel and maintenance
Light microscopy	Magnification technique	Time consuming, requires skilled personnel and high maintenance

The methods mentioned in Table 1.1 above are highly sensitive and accurate in the detection of Malaria, however, it must be noted that they all require highly trained personnel, a laboratory environment to keep and maintain them, and some are time consuming. Therefore, they are not useful at point-of-care for detection of Malaria in low infrastructure settings, and in places like rural areas, where laboratories are nowhere to be found and clinics are not available.

Table 1.2: Methods that have been used to detect Malaria using Lateral flow approach.

Size of AuNPs	Antibody	Analyte	Reader	Limit of Detection	Linear Dynamic Range	Refs
14 nm	IgG	pLDH	Smartphone	10 ng.mL^{-1}		Present work
40 nm	(Anti-mouse) Monoclonal Anti-hemoglobin (IgG1)	Hemoglobin	Naked Eye	42.5 µg.mL^{-1}	20 – 130 mmol.moL^{-1} (4 – 14%)	(Ang *et al.* 2016)
30 – 40 nm	Biotinylated DNA	HIV-1 DNA	Naked Eye	0.24 pg.mL^{-1}	8 – 64 ng.mL^{-1}	(Fu *et al.* 2016)
40 nm	Mycobacterium Tuberculosis Antib (38 kDa monoclonal antibodies)	Mycobacterium Tuberculosis	Naked Eye	5 ng.mL^{-1}	10 – 300 ng.mL^{-1}	(Mdluli *et al.* 2014)
15 nm	Nitrilotriacetic Acid	Malaria biomarker recombinant PfHRP-	Naked Eye	2000 parasites.µL^{-1}	0 – 40 nM	(Gulka, Swartz and Wright

		2				2015)
10 & 40 nm	Biotin /streptavidin	Troponin & Mayoglobin	Cell phone & home scanner	1 $ng.mL^{-1}$	(No data)	(Mak, Beni and Turner 2016)
NR	Proteins	Rabbit IgG	Google glass & Smartphone	10 $pg.mL^{-1}$	(No data)	(Quesada-González and Merkoçi 2015)
NR	Monoclonal capture (anti-hCG α Mab)	hcG	Smart phone	0.20 $\mu g.mL^{-1}$	0.28 – 0.40	(Wong *et al.* 2015)
40 nm	Goat anti-mouse IgG capture antibodies	PfhRP-2	Smart phone	0.966 nM	0 – 30 nM	(Scherr *et al.* 2017)

NR	Ni-NTA Malaria capture antibodies	PfhRP-2	Smart phone	< 1 parasite.µL^{-1}	25 – 250 µL	(Ricks *et al.* 2016)
NR	Malaria capture antibodies		Smart phone & bare eyes	20.6 parasites.µL^{-1}	0 – 500 parasites.µL^{-1}	(Scherr *et al.* 2016)
		Malaria				
14 nm	IgG (Anti-mouse)	pLDH	Smartphone	10 ng.mL-1		Present work
40 nm	Monoclonal Anti-hemoglobin (IgG1)	Hemoglobin	Naked Eye	42.5 µg.mL^{-1}	20 – 130 mmol.mol^{-1} (4 – 14%)	(Ang *et al.* 2016)
30 – 40 nm	Biotinylated DNA	HIV-1 DNA	Naked Eye	0.24 pg.mL^{-1}	8 – 64 ng.mL^{-1}	(Fu *et al.* 2016)

40 nm	Mycobacterium Tuberculosis Antib (38 kDa monoclonal antibodies)	Mycobacterium Tuberculosis	Naked Eye	5 $ng.mL^{-1}$	10 – 300 $ng.mL^{-1}$	(Mdluli *et al.* 2014)
15 nm	Nitrilotriacetic Acid	Malaria biomarker recombinant PfHRP-2	Naked Eye	2000 $parasites.\mu L^{-1}$	0 – 40 nM	(Gulka, Swartz and Wright 2015)
10 & 40 nm	Biotin /streptavudin	Troponin & Mayoglobin	Cell phone & home scanner	1 $ng.mL^{-1}$	(No data)	(Mak, Beni and Turner 2016)
NR	Proteins	Rabbit IgG	Google glass & Smartphone	10 $pg.mL^{-1}$	(No data)	(Quesada-González and Merkoçi 2015)
NR	Monoclonal capture (anti-hCG α Mab)	hcG	Smart phone	0.20 $\mu g.mL^{-1}$	0.28 – 0.40	(Wong *et al.* 2015)

40 nm	Goat anti-mouse IgG capture antibodies	PfhRP-2	Smart phone	0.966 nM	0 – 30 nM	(Scherr *et al.* 2017)
NR	Ni-NTA Malaria capture antibodies	PfhRP-2	Smart phone	< 1 parasite.μL^{-1}	25 – 250 µL	(Ricks *et al.* 2016)
NR	Malaria capture antibodies	Malaria	Smart phone & bare eyes	20.6 parasites.μL^{-1}	0 – 500 parasites.μL^{-1}	(Scherr *et al.* 2016)
14 nm	IgG (Anti-mouse)	pLDH Hemoglobin	Smartphone	10 ng.mL^{-1}		Present work
40 nm	Monoclonal Anti-hemoglobin (IgG1)	HIV-1 DNA	Naked Eye	42.5 µg.mL^{-1}	20 – 130 mmol.moL^{-1} (4 – 14%)	(Ang *et al.* 2016)

30 – 40 nm	Biotinylated DNA		Naked Eye	0.24 pg.mL^{-1}	8 – 64 ng.mL^{-1}	(Fu *et al.* 2016)
40 nm	Mycobacterium Tuberculosis Antib (38 kDa monoclonal antibodies)	Mycobacterium Tuberculosis	Naked Eye	5 ng.mL^{-1}	10 – 300 ng.mL^{-1}	(Mdluli *et al.* 2014)
15 nm	Nitrilotriacetic Acid	Malaria biomarker recombinant PfHRP-2	Naked Eye	2000 parasites.µL^{-1}	0 – 40 nM	(Gulka, Swartz and Wright 2015)

NR: Not reported; IgG: Immunoglobulin G; pLDH: Plasmodium lactate dehydrogenase; PfhRP-2: *Plasmodium* falciparum histidine rich protein – 2; HIV: *human immunodeficiency virus;* hcG: Human chorionic gonadotrofin

Molecular biology methods are common methods used in biochemistry, molecular biology, genetics and biophysics involving analysis and manipulation of DNA, RNA, lipid and protein. They have been successfully applied in studies of various diseases and conditions, in the study of mycobacterium tuberculosis (Brossier *et al.* 2017), identification of molecular targets in vulva cancer (Palisoul *et al.* 2017), molecular signatures in breast cancer (Lal *et al.* 2017), direct anharmonic correction method by molecular dynamics (Liu *et al.* 2017), molecular constituents of blood-brain barrier (Chow and Gu 2015), and in shock waves simulated using the dual domain material point method combined with molecular dynamics (Zhang and Dhakal 2017). The polymerase chain reaction (PCR) is a method that makes copies of a DNA sequence with repeated reactions with polymerase and, is one of the molecular methods commonly used in studies of malaria. PCR is a powerful diagnostic tool with many advantages such as reliability, high sensitivity, easy operation and cost efficiency (Garafutdinov, Galimova and Sakhabutdinova 2017). In malaria diagnosis, PCR has been applied for severity and parasite load using microscopy ($p<0.001$) and quantitative PCR (0.001), where quantitative PCR was found to be useful in predicting the outcome (Dormond *et al.* 2015). Although quantitative PCR might be best, it suffers major drawbacks of requirement of skilled personnel, electricity and a specialized controlled environment.

A lot of people die from malaria every day since symptoms manifests as flu and other less harmful diseases, hiding the extent of the infection leading to fatality, yet it is prevented if early diagnosed. A quick, reliable and convenient way to detect malaria is therefore required to minimize deaths in this daily technology era. In this study, we report a novel rapid testing kit for malaria, *plasmodium falciparum histidine rich protein-2*, by detecting *plasmodium lactate dehydrogenase (pLDH)*, pLDH is a glycolytic pathway enzyme which is produced by the different Plasmodium species, but it carries species-specific isomers (Harani; *et al.* 2006). The pLDH enzyme is destroyed by immune system within 24 hours of effective malaria post-treatment (Oduola *et al.* 1997). It is therefore without any doubt that pLDH antigen is mainly considered as a specific biomarker for the presence and detection of the early presence of

Plasmodium in blood, and could be used for screening of malaria infection in malaria-endemic countries. We have embedded Quick Response technology coupled with Google Analytics enable our devices to be used to demonstrate the real time monitoring and screening of malaria.

1.1 Malaria methods of analysis

There are a number of techniques that successfully detect malaria in blood samples. The detection techniques include; Aptamer-mediated *Plasmodium*-specific diagnosis of malaria (Cheung *et al.* 2017), a highly sensitive and selective malaria detection electrochemical biosensor based on aptamer with adjustable dynamic response range (Figueroa-Miranda *et al.* 2018), microfluidic loop-mediated isothermal amplification array for detection of malaria-related parasites and vectors (Mao *et al.* 2018), and the molecular detection of malaria parasite (Gupta *et al.* 2016). This study however focused on the major methods which are polymerase chain reaction (PCR) and microscopy. A list of other methods is presented above in Table 2.

1.1.1 Polymerase Chain Reaction (PCR)

The polymerase chain reaction technique is a useful tool and has done great work in understanding of diseases fatal to communities, cities, countries and the world. The PCR has made it feasible to study the genetic diversity of parasites in small samples of infected blood, supporting extensive surveys of natural parasites population to be conducted, in addition the technique is applicable in mosquito stages of malaria parasite allowing direct assessments of the frequency of crossing between parasite clones in nature (Babiker and Walliker 1997).

1.1.2 Microscopy

Microscopy is a method recommended on a study of rapid diagnostic tests for malaria parasites, for microscopic examination of stained thin and thick blood films, it can detect 50 parasites.μL^{-1} (0.001 parasitemia) (Moody 2002).

Types of microscopy techniques include light microscopy, a highly quantitative method available in individual laboratories and often centralized in core facilities. However, although quantitative microscopy is becoming a customary tool in research, it is rarely standardized and to achieve accurate quantitative microscopy data and reproducible results, three levels of standardization must be considered; (1) the sample, (2) aspect of the microscope, and (3) the detector (Deagle, Wee and Brown 2017). It serves as a versatile technique applicable in many fields of study and has been applied in the diagnostic pathology of Alzheimer's disease from routine microscopy to immunohistochemistry, and experimental correlations (Nuovo *et al.* 2017), on *in-vivo* confocal microscopy of corneal nerves in health and disease (Cruzat, Qazi and Hamrah 2017), and in malaria, the light emitting diode (LED) fluorescence microscopy has been used for accurate, rapid diagnosis and LED fluorescence microscopy is moderately sensitive and highly specific in comparisons with light microscopy (Hathiwala *et al.* 2017), and scanning electron microscopy (SEM) promises easy detection and revealed that erythrocytes infected with plasmodium falciparum, the human parasite display knob like structures on their surface comprising parasitized proteins (Hayakawa and Matsuoka 2016).

1.2 Biomarkers for malaria detection

Proteins are polymer chains made of amino acids that are linked together by peptide bonds, they are known to be building blocks of body tissue, can also serve as fuel source, and are also essential nutrients to the body. Proteins are applicable in a lot of research fields entering as the biological material and studies involving proteins have been undertaken until present. Le Zhang and co-workers studied the protein to protein interactions which revealed generic patterns of ion-specific perturbation for phase behaviour of chimeric fusion protein (Zhang *et al.* 2017), crucial protein study involving lipid metabolism reported protocols and pitfalls in obtaining fatty acid binding proteins for biophysical studies of ligand-protein and protein-protein interactions (Wang *et al.* 2017), and a study focused on nutrient composition and protein profile of a

range of rice protein ingredients containing 32 – 78% total protein using sodium dodecyl sulphate polyacrylamide gel electrophoresis (SDS-PAGE) and size exclusion high performance liquid chromatography (SE-HPLC) (Amagliani *et al.* 2017). The significance of protein studies has grown since they are important molecules in our daily lives in food, health and research world.

1.2.1 Plasmodium falciparum histidine rich protein – 2

Plasmodium falciparum histidine rich protein – 2 is a type of malaria protein responsible for the millions of human deaths across the globe. A lot of research focused on *plasmodium falciparum histidine rich protein – 2* (PfHRP - 2), the fatal malaria protein, however, there still is a need for better developed technological methods to address the malaria challenge. A debate on the population genetic structure of malaria parasites assisted through studies that addressed critical issues and techniques to efficiently detect and view the parasite, the PCR served a critical role, knowledge generated assist in future developments of antimalarial drugs and possible malaria vaccines (Babiker and Walliker 1997). Li and co-workers investigated the genetic diversity of the (PfHRP – 2) gene in clinical parasite isolates collected in recent years from the china-Myanmar boarder area (Li *et al.* 2015), and realised (PfHRP – 2) based rapid test kits would be affected by deletion of the *Plasmodium falciparum* reticulocyte-binding protein homolog 5 (PfHRP – 2) gene. The owl monkey serves as a vital tool in research to develop drugs and vaccines against human *falciparum* malaria. However, many *plasmodium falciparum* parasites are unable to invade nancymaae erythrocytes rendering non-infective to monkeys, and (PfHRP – 2) gene is successfully utilized in research to invade owl monkey and rats erythrocyte (Hayton *et al.* 2013). According to literature, *Plasmodium falciparum* is not the only deadly human malaria existing, *plasmodium knowlesi* is the fifth malaria type which is like falciparum, is life threatening. The knowlesi parasite has only been reported in Southeast Asia, and is important but overlooked (Yegneswaran, Alcid and Mohan 2009). *Plasmodium falciparum* is generally susceptible to artemisinin derivatives but a reduction in susceptibility occurs in areas where the drug has been used for a prolonged time period

(Henglin *et al.* 2003). *Plasmodium falciparum* has a central enzyme called hypoxanthine – guanine phosphorybosyltransferase (HGPRT) which is potential antimalarial chemotherapeutic target also salvage to the pathway for purine nucleotide biosynthesis. There is an existing difference between human and malarial HGPRT which can be exploited in the design of a specific inhibitor for this enzyme (Sarkar, Ghosh and Datta 2004). *Plasmodium falciparum lactate dehydrogenase* is a key enzyme for malarial parasites energy generation. *Plasmodium lactate dehydrogenase* (pLDH) is the terminal enzyme of anaerobic Embden-Meyerhoff glycolysis, plays an important role in human malaria parasites carbohydrate metabolism (Basco *et al.* 1995). Markwalter and co-workers reported a sensitive, magnetic bead based coulorimentric assay for *Plasmodium falciparum lactate dehydrogenase* extraction and purification from blood matrix based on antigen binding to antibody-functionalized magnetic particles (Markwalter, Davis and Wright 2016), while Jain and co-workers in an attempt to discover better detection technique for malaria, developed a graphene oxide-aptamer sensor for pLDH capable of detecting as low as 0.5 fM pLDH (Jain *et al.* 2016).

1.2.2 Protein

Bovine Serum Albumin (BSA), a serum protein derived from cows often used as a protein concentration standard in lab experiments. It is a useful protein in research, with a number of discoveries that have been made through it. Its application is not limited to biology but extends to other fields of study and still affords researchers quality work and novel discoveries. The protein is a less dense semi-powder or granules, white in colour and dissolves 100% in H_2O. BSA was found to be compatible with many metals enabling new detection techniques to be concluded. Shuang Zhao and co-workers developed a BSA-AuNCs based enhanced photoelectrochemical biosensor and studied its potential use in multichannel detection (Zhao *et al.* 2017), after enhancement realised improvement on LODs from 325 µM to 25 µM (H_20_2) and from 7.45 µM to 1.5 µM (Dopamine), Ana E. Ledesma successfully applied BSA in modifying a ZnO nanoparticle for spectroscopic characterization and docking studies,

increasing BSA denaturalization from 57 to 65 ^{0}C (Ledesma *et al.* 2017), Ajou University researchers Jin-Seok Choi and Nilesh Meghani, on a cancer study investigated the impact of surface modification in BSA – nanoparticles for uptake in cancer cells and found the uptake of modified poly allylamine hydrochloride – BSA NPs to be 2 times higher than that of unmodified BSA – NPs (Choi and Meghani 2016), while Carlos Muňoz-Bustos and team used BSA to coat copper nanoclusters and developed a simple, rapid and cost effective novel fluorescence sensor for mangiferin sensitive and selective detection (Muñoz-Bustos *et al.* 2017). On a spectroscopic analysis of interaction of BSA with toluidine blue and its sosodynamic damage under ultrasonic irradiation, they found that toluidine blue (TB) can bind to BSA molecules and the synegertic effects of TB and ultrasonic irradiation effects can efficiently damage the BSA molecules (Wang *et al.* 2011). Bovine serum albumin minimizes aggregation of nanoparticles (Leopold *et al.* 2017), and works well in lateral flow binding to gold nanoparticles.

1.2.3 Human Serum Albumin

Human serum albumin (HSA) is a protein found in human blood, produced by the liver and it is the most abundant protein in human blood plasma. It is a protein that has been used extensively in research for binding and aggregation of substrates (Singla *et al.* 2017). Mahdi Kavoshchian and co-workers used I as an immobilizer in a novel polymeric metrix as an alternative sorbent in hemoperfusion columns for bilirubin removal (Kavoshchian *et al.* 2015), Mesken J. and team on a study to modify plasmid-loaded HSA nanoparticles with cell penetrating peptides – cellular uptake and enhanced delivery, were able to demonstrate that nanoparticles can be produced with a different peptide surface modifications (Mesken *et al.* 2017), it enhances the accumulation and retention of anti-tumor drugs (Kujda, Adamczyk and Ciesla 2016). On an anticancer study of binding interactions, it was discovered that HSA binds to clofarabine, an important anticancer drug at 298 K with binding constant of 4.120×10^{3}, I bind to clofarabine near drug site II and hudrophobic interactions and hydrogen bonding are main forces (Ajmal *et al.* 2017).

1.2.4 α 1-Acid Glycoprotein

Alpha 1-Acid Glycoprotein (AGP) is an acute phase plasma alpha – globulin glycoprotein modulated by two polymorphic genes. An ELISA to measure porcine AGP in pig plasma was developed, and is a highly glycosylated mammalian acute-phase protein which is synthesized primarily in the liver and represent the major serum protein in newly born pigs (Caperna *et al.* 2015). On a potential lung cancer biomarker study, sandwitch ELISA quantified high serum levels of Alpha-1-acid Glycoprotein while one way ANOVA analysis predicted highly significant variation of Alpha-1-acid Glycoprotein among all types studied (Ayyub *et al.* 2016). Investigation of interaction of newly approved kinase inhibitors Cabozantib (CBZ) and Tofacitinib (TFB) with human Alpha-1- acid Glycoprotein under simulated physiological conditions where protein binding caused alterations to tertiary structure and hydrogen bonding and hydrophobic interactions occur between CBZ and AGP while TFB only has hydrophobic interactions (Ajmal *et al.* 2016). On a study of binding interaction between clofarabine with Human serum albumin and AGP the two proteins found in human plasma, clofarabine was found to bind at 298 K with AGP at 8.128×10^3 binding constant and observed is a stronger interaction between AGP and clofarabine (Ajmal *et al.* 2017).

1.2.5 Lipoproteins

Lipoproteins are a set of nanoparticles whose main role is fats transportation in the body. They are biocompatible, biodegradable, non-immunogenic and naturally are targeted to some disease sites (Thaxton *et al.* 2016). They provide active mobilization of endogenous and exogenous (dietary) lipids through aqueous compartments between cells and in blood and body tissues where lipid molecules can either utilised as an energy source or stored (Aru *et al.* 2017). A lot of studies have been conducted on lipoproteins, Robert E. Heinl and co-workers reviewed a pathophysiological model of lipoprotein-X syndrome from two medical centres related to three cases in the United states (Heinl *et al.* 2017). Serum lipoproteins undergo different chemical modifications impacting their normal functions, low density lipoproteins are made more proatherogenic

through modifications such as oxidation, glucooxidation, carbamylation and glycation (Chistiakov *et al.* 2017). In high risk atherosclerosis patients, specific lipoprotein apheresis began to be used in the 1970's with homozygous familial hypercholesterolemia and elevated lipoprotein levels, thus apheresis is capable of reducing by more than 80% cardiovascular events in patients with high Lipoprotein levels (Julius 2017). Since atherosclerosis is a chronic and progressive disease which leads to coronary heart disease, stroke and atherosclerotic cardiovascular disease (ASCVD), previous investigations showed an atherogenic role of oxidized low density lipoprotein (ox-LDL) in progression of ASCVD, Shen Gao and Jing Liu so a need to review the atherogenic mechanism of ox-LDL, the method of measuring ox-LDL in the circulation, lifestyle modification on ox-LDL level, effect of medical therapy, association between circulating oc-LDL and therosclerosis, including sub-clinical atherosclerosis and clinical ASCVD events in observational studies (Gao and Liu 2017). Lipoprotein is an important protein in the body and health of humans.

In malaria early stages, lipoprotein plays a vital role, hence major lipoprotein conducts the dynamics of lipid metabolism in hemolymph of the mosquito and it was discovered that malaria parasite undergoes lipid uptake while in the vertebrae host (Atella *et al.* 2009). A cohort study of plasmodium vivax in acute and convalescent phase measured serum concentrations of triglycerides, total cholesterol, low-density lipoprotein and high-density lipoprotein. Serum total LDL, HDL and cholesterol were low and high triglycerides in the acute phase, and observed a transient change in lipid profile between convalescent and acute stages which many be useful in clinical analysis for treatment of plasmodium vivax (Mesquita *et al.* 2016).

1.2.6 Plasma

Blood plasma is a component of blood that normally holds the blood cells in whole blood suspension. Blood is a complex colloidal system containing large numbers of small and large biological components like proteins, minerals and carbohydrates along with cells and therefore it is utilised in various diagnostic

tests as a sample of high potential. However to achieve better results, it is highly advisable to reduce the avoidable complexity of blood sampling by separating cells and to use plasma or serum sampling (Tiwari, Garnier and Rao 2017). Blood plasma contains components such as proteins, hormones, ferments, electrolytes, waste products, minerals, glucose, clotting factors etc, however proteins are the main component of the plasma (Mona *et al.* 2013). One study conducted in Indonesia based on Glutathione (GSH) and oxidized Glutathione (GSSG) as well as plasma concentration of albumin revealed that the average plasma Glutathione GSH and GSSG level also plasma GSH/GSSG ratio in both the uncomplicated and complicated malaria are similar and plasma concentration of albumin is lower than normal in both groups (cvFitri *et al.* 2016). Studies involving plasma have gone deeper in the quest to finding malaria cure; Brazilian researchers investigated effect of age on Mefloquine concentrations in erythrocytes during the acute phase of falciparum malaria; and found no age effect of patient age on the steady – state concentrations of Mefloquine in the plasma and erythrocytes (Vieira *et al.* 2016), on a search to understand another malaria infection of the cerebral fatal mostly to children, a United Kingdom based study revealed that it involves a severe neurological complication of in children and adults. A study conducted on mice, results indicated acute – phase reaction and co-agulation cascade activation and leakage of plasma proteins into the brain appeared as a sign of neurological response (Moussa *et al.* 2017).

1.3 Quick Response Codes

Quick response (QR) codes have gained popularity in the research and development field, modifying tedious processes to simpler and faster. Studies have been conducted on quick response codes leading to fascinating discoveries and radical improvement of systems, Jamu and co-workers studied the utilization of QR codes for multi-professional learning in clinical practise (Jamu, Lowi-Jones and Mitchell 2016), while Kim and Woo utilized the Technology Acceptance Model (TAM) to study consumer acceptance of QR code system in food traceability (Kim and Woo 2016), a South Korea based

study. Further studies examined and explored more applications of QR codes to ease public lives. Government services are also to benefit from QR codes hence a study to enhance government services using QR codes has been conducted, a study aimed at minimizing costs and maximizing utility of services to taxpayers (Lorenzi *et al.* 2014), in geology, land usage studied a virtual tour of geological heritage valourising heritage using Google earth and QR code (Martínez-Graña, Goy and Cimarra 2013). As far as smartphones and QR code scanners are a vital tool in QR code scanning, QR codes enjoy great versatility finding relevant application across all industries and study fields. The world's continuously upgrading of technology, information security has become more important, encryption using QR code was successfully studied (Wang *et al.* 2014). As mobile technologies are booming, QR codes are becoming part of our lives, being used for various purposes, Turkish researcher Demir and team found QR codes more likely to be used for mobile marketing in future (Demir, Kaynak and Demir 2015).

Figure 1.1: QR codes created from a website link. The above barcodes when scanned should direct the user to a corresponding website.

QR codes as shown in Figure 1 above contain three similar squares positioned at each corner of the code. These squares are a critical part of the code's active and deactivation, hence blocking of the small boxes deactivates the code. The principle of cutting out a small piece of the corner and replace it with a test and control reaction band provided a unique strong approach in the digitization and encoding of medical diagnostics.

1.4 Google Analytics

Google Analytics is a tool offered by Google to assist in statistical data tracking and website performance monitoring. Website monitoring is on the increase and analytics offers the best option to tracking of website visitor statistics and performance (Plaza 2011; Gunter and Önder 2016). Google analytics application is not limited to the current discoveries and developments but can be stretched to serve a wide spectrum, in traffic monitoring of city arrivals (Gunter and Önder 2016), social media campaigns (Gordon, Shand and Black 2016), quantifying potential tourist behaviour (Padhi and Pati 2017).

Google is the most popular search engine that covers nearly 90% of online searches used by both physicians and patients to obtain health information (Del Pizzo *et al.* 2016). A study revealed that curiosity, concern as well as motivation to increase knowledge as a deep motive for people to search the internet for health related answers.

1.5 RGB values and Color

RGB is an abbreviation for the three colors, red, green and blue. It is a color system in which all three are added together to form various colors, and it is thus referred to as a RGB color model. It can be used to determine any color existing. Italian researcher Pizzo and co-workers have used the traditional RGB camera and depth sensor as acquisition technology to count the number of people crossing a virtual line (Del Pizzo *et al.* 2016), while Hirayama and co-workers studied the effect of low concentrations of Irgarol 1051 on RGB (red; green; blue) colour values of the hard-coral Acropora tenuis (Hirayama *et al.* 2017). As RGB values increase, they move towards the white end of the spectrum as concentration of Irgarol 1051 increased (Hirayama *et al.* 2017). In the study of domain adaptation from RGB – D to RGB image, Li and co – workers evaluated their novel method and found it useful since discrepancy between source and target data can be incorporated with classifiers of source and target data (Li *et al.* 2017). Tahoun and co-workers investigated modified RGB-based kerogen maturation index (KMI): Correlation and calibration with

classical thermal maturity indices, and found the newly modified, RGB-based maturation index called Kerogen Maturity Index (KMI) to confidently and effectively detect subtle and progressive changes in kerogen maturation with depth (Tahoun *et al.* 2017). The RGB value has been extensively used in various application such as in a study conducted in China, RGB value in rice used to study modelling dynamics of leaf color (Zhang *et al.* 2014). Hypertext markup language (HTML) is a complicated code that expresses a RGB value in a code form. HTML codes are more complicated than RGB, can be difficult to learn and frustrating (Mauriello, Pagnucci and Winner 1999). In this study we use RGB to determine color and concentration of AuNPs.

1.6 Problem Statement

Malaria continues to be a serious challenge in endemic regions, taking lives every year. The ambiguity of malaria symptoms resulted in a disastrous number of hospital emergencies, and more than symptoms, the methods of malaria detection have not addressed the concept of time it takes to submit results before medication can be dispatched to people, accuracy, improvement and demographics. This study presents novel rapid malaria diagnostic technique capable of reporting and transferring real-time monitoring of disease prevalence data using traditional testing kits coupled with QR codes and encoded with Google analytics tracking.

1.7 Aim of Study

To develop a novel gold nanoparticle based rapid test kit with QR code and Google Analytics technology advancement.

1.8 Objectives of Study

- Preparation, synthesis and conjugation of AuNPs for use in lateral flow development.

- Assemble a lateral flow immunoassay utilizing malaria antigen(Ag) and plasmodium lactate dehydrogenase antibodies.
- Decode, angle optimization and coupling of QR codes with the traditional malaria immunoassay.
- Detect malaria, and real–time data transfer for disease surveillance studies.

1.9 Dissertation outline

This dissertation contains four chapters, and is presented as follows:

Chapter 1

This chapter contains the introduction, problem statement, aim and objectives of this study.

Chapter 2

This chapter contains the reagents used, the instruments that were utilized and all methods that involved in generation of results. Details of chemicals and the appropriate suppliers, instrumentation and analysis including UV-Vis and TEM, synthesis and stabilization of AuNPs, preparation of antibody-gold conjugate, color determination using RGB values, preparation of lateral flow strips, assembling of lateral flow test strips, and the data analysis and tracking. This chapter briefly expands on experimental procedures carried out in this study.

Chapter 3

This chapter outlines the results and discussion of all studies undertaken. The characterization of AuNPs, flocculation using BSA protein and optimization of salt content studies are reported. Color determination using RGB values, optimization of antibody concentrations, the fabrication of QR codes, scanning distance optimization and Google Analytics tracking of developed websites are reported and discussed in this chapter. The most

important and key information of the current research is briefly explained in this chapter.

Chapter 4

This chapter outlines the conclusions, recommendations and some of the important achievements of this study.

CHAPTER 2

Experimental

2. Experimental

2.1 Reagents and Chemicals

Tween 20, sucrose, tri-sodium citrate ($Na_3C_6H_5O_7$), bovine serum albumin (BSA) and Anti-mouse IgG (a secondary antibody) was purchased from Sigma-Aldrich (SA). Anti-*Plasmodium lactate dehydrogenase* (pLDH) antigen was purchased from Vista diagnostics and CTK Biotec, respectively (Kirkland, WA, and California). All buffer solutions were made in high purity water obtained from the Milli-Q water purification system purchased from Millipore (Bedford, MA, USA). The nitrocellulose membrane Whatman AE98, wick/sample pad GB002, conjugated pad, 60 x 300 mm- MIBA-020 backing support and chromatographic paper were all purchased from Diagnostic Consulting Network (DCN, California, USA). The antibody was conjugated to colloidal gold particles (14 nm), resulting in colloidal gold labelled antibodies.

2.2 Instrumentation and Analysis

The instruments used in this study are explained with chemicals and all consumables that were utilized. Characterization of nanoparticles and protein conjugation were monitored using the below.

2.2.1 Ultraviolet – Visible Range

Optical measurements were performed with Lambda 35 UV-Vis spectrophotometers supplied by PerkinElmer (Durban, South Africa). The analysis were done in quartz cuvettes (1 cm, path length), using conductivity water as a reference solvent sample which was purified using a Hettich MIKRO 22R centrifuge. Absorption spectra of AuNPs were recorded on a Lambda 35 UV-Vis spectrometer. The maximum absorption wavelength was determined by calculating the wavelength at which

$$\frac{dA}{d\lambda} = 0 \qquad (1)$$

Where *A* = absorbance and λ = absorption wavelength

2.2.2 Transmission Electron Microscopy (TEM)

Transmission electron microscope (TEM) images were obtained using a JEM-2100F at 200 kV. The TEM grids were prepared by depositing approximately 10 µL of the solution obtained after centrifugation and allowed to dry in air. The immobilization of proteins at a rate of 1 µL cm^{-1} and the conjugate at 10 µL cm^{-1} was performed with a Biodot XYZ Series dispensing system supplied by Biodot (USA). ESI Quanti reader, a lateral flow studio capable of collecting data of the strips with the dimension of 5 mm (breath) and 10 cm (length) was used to determine the lines' intensities.

2.3 Preparation of Antibody-Gold conjugate

Colloidal AuNPs with a mean diameter of 14 nm were synthesized using the sodium citrate method (Philip 2008; Oyeyemi *et al.* 2016). The optimum concentration of antibodies for conjugation was determined using flocculation (Piper *et al.* 1999). Briefly, 200 µL of antibody was added to 20 mL citrate stabilized AuNP solution and the mixture was gently stirred for 10 min. Then 3 mL of 1% (w/v) BSA solution was added to the mixture and continued stirring for 30 min. Thereafter, the solution was centrifuged at 15 000 rpm for 45 min, and suspended in 4 mL dilution buffer (20 mM Tris/HCl buffer (pH 8.2)). 10% (w/v) BSA was added as a blocking agent. In order to determine the optimum attachment of antibody on the surface of AuNPs, flocculation was conducted and evaluated using UV-Visible spectrophotometer. A detailed synthesis of AuNPs is described below.

To synthesize gold nanoparticles, 0.3033 g of hydrated Auric tri-chloride monohydrate ($AuCl_3H_2O$) was dissolved in a 1 L volumetric flask containing deionized water, after all dissolved; it was then topped to the mark using deionized water. The dissolved gold salt was transferred into a 1000 mL, heated to boiling until a yellow colour was observed. A 100 mL of 0.04 M sodium citrate solution was slowly added to the boiling solution and stirring initiated. On

constant stirring, the solution turned dark (black) and in 5 minutes turned to pink. The synthesis was followed citrate reduction of AuNPs adopted from Turchvich method (Agunloye, Gavriilidis and Mazzei 2017).

Preparation of the gold – antibody was achieved through adding 1 mL of 10% (m/v) BSA to 5 mL AuNPs, and homogenized by shaking. To the above solution 0.1 mL of the antibody was then added. A colour change to dark red observed a few minutes.

2.4 Color Determination Using RGB

The RGB values were generated by the online RGB generator software. The RGB generator uses three major colors to determine the right color of an uploaded picture.

To generate the RGB values, the following the steps were done:

- Capturer a photo of the colour of a solution
- On the internet, open RGB online generator
- Then upload the captured image
- Click on the part of the image that represents the color of the whole solution or image. You will have RGB, HTML codes and HSV.
- HTML and HSV are generated
- Proceed with data analysis using other software such are excel

2.5 Preparation of lateral Strip

The conjugate pad was first treated with phosphate buffer saline (PBS) containing 5% sucrose (w/v), 0.5% tween 20 and 1% (w/v) BSA and dried in an oven for 30 min. This was followed by applying the colloidal gold-pan-malaria pLDH (O.D. 10) to the conjugate pad and oven dried for 30 min. Anti-pf pLDH and anti-mouse IgG were spotted on the test and the control line, respectively, on the nitrocellulose membrane with 0.1% (w/v) BSA and then drying again. The prepared nitrocellulose membrane, absorption pad and sample pad were

assembled and attached on the backing support. Approximately 30 µL of the recombinant pLDH (Au) sample was pipetted into a reaction holder to see the results of the test strip based on the colorimetric lines. Fig.2.1 below shows the prepared lateral flow strip.

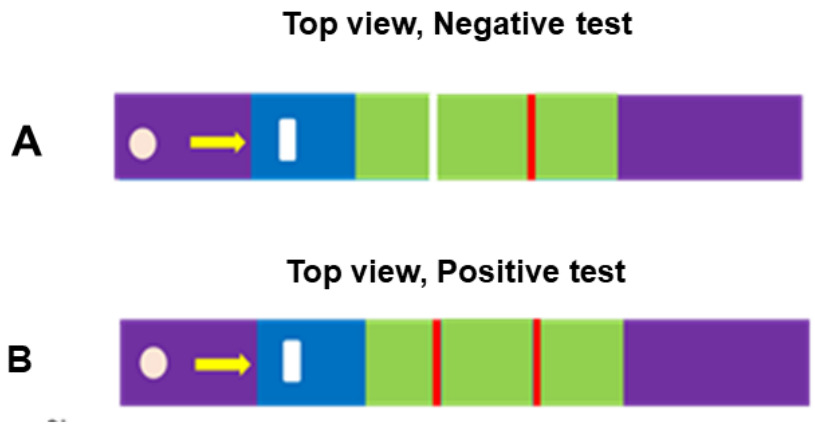

Figure 2.1: The sketch design of the commonly used lateral flow test kit, one showing a (A) no reaction on the test (white) line and a reaction on the second (red line), (B) shows a similar assembly of the lateral flow with two red lines one on test position and one on control position which depicts a positive test.

2.6 Assembly of lateral flow test strips

The prepared sample containing a recombinant antigen (pLDH) was pipetted into the well of the cassette, and the sample of the recombinant antigen standard was allowed to flow over the sample pad by capillary flow and captured by the test line as shown in Fig.2.2. The immobilized colloidal gold-labelled anti-bodies, which are re-suspended by applying buffer solution, react with the antigen (if it is detected in the sample extract), which becomes an analyte-detector complex. The analyte-detector complex continues migrating up the membrane to the test line and the control line. In cases where the antigen is not present in the sample, the analyte-detector complex will pass the test line and react with the immobilized secondary antibody (control line); hence, one line will be observed (negative results). If the antigen is present, the analyte-detector complex will bind to the immobilised antibody and the secondary antibody on the nitrocellulose membrane showing two lines (positive results). If

no control line is present, the test is considered to be invalid. The appearance of two pink lines (test and control) meant that the sample contains the antigen. This procedure is somewhat similar to the previously reported and improved dual lateral flow diagnostic assays for the detection of the antigen for tuberculosis (Turkevich, Stevenson and Hillier 1951). A variety of concentrations of samples (10, 50, 100, 200 and 300 ng.mL^{-1}) with the antigen (pLDH) for validity tests were prepared.

2.6

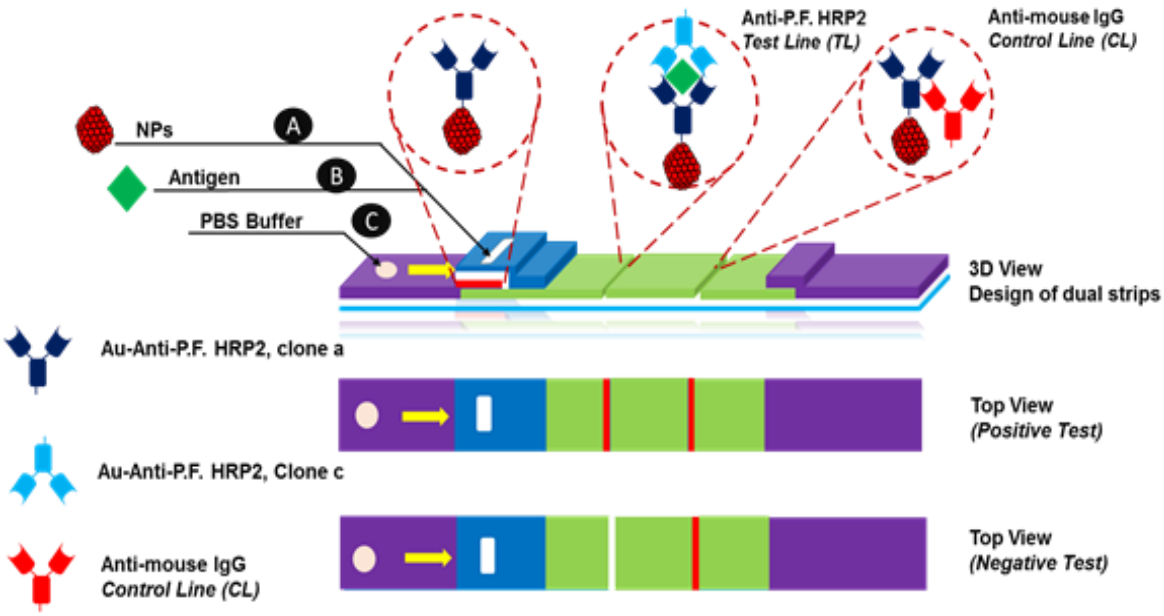

Figure 2.2: Sketch design of a lateral flow and labels of each section. (A) BSA flocculated AuNPs conjugated to a universal anti-body are deposited onto wik pad, (B) Antigen from the sample (blood) is deposited, (C) PBS buffer is introduced on the white circle to improve capillary action.

2.7 Data Analysis and Tracking

The QR code scanning software was downloaded on a cell phone (Samsung J1 ACE) to confirm the valid and invalid scan patterns and orientation of QR codes. QR code scanner installed in a smartphone was used. An optimized distance was kept between 180 and 210 mm for scanning device from the test kit. All lateral flow QR code devices were sent to independent testing stations that are located at various geographical positions such as Brazil, the United

States, Belgium, Latvia, Canada, Russia, Italy and Mozambique. Then, report was generated which showed the accessible detailing of the time, continent, country, city and true geographic testing location and included whether the test was positive, negative or invalid. Data analysis involved smart phones, QR codes, QR code scanning software and Google analytics.

2.8 Fabrication of QR codes

The QR codes created on a website were aligned such that they fit the test kit size, and then printed on an A4 paper. After printing on paper, the QR codes were attached manually onto the test kit.

The QR codes were modified as follows:

- One QR code was decoded on the corner in top left square box and the second was decoded on two opposite square corner boxes. The last code decoded on one corner square box.
- The decoded parts of the QR codes were then overlaid to form a flowing mechanism.
- The overlaid codes were transferred to assembled testing kits and the decoded parts aligned to deposited antibody such that when a sample is run, the control and test lines appear on the decoded part of the codes.
- The kits were covered with its closing materials.

:

CHAPTER 3

Results & Discussion

3. Results & Discussion

A Google analytics QR technology enhanced for lateral flow which is applicable for on-site diagnosis of malaria *Plasmodium lactate dehydrogenase* (pLDH) has been successfully developed. This diagnostic assay has brought, in the diagnostics field, a new technology upgrading the current diagnosis methods and increasing results coverage through Google analytics tracking technology. This was successfully demonstrated through various trials and tests for its effectiveness to enable an on-site detection as well as to generate demographics, statistical evaluation of population and thus, decreasing the turnaround time between diagnosis and results transfer to authorities and advanced laboratories in order to speed up treatment initiation. This study shares light on diseases in South Africa and other sub – countries in the context of diagnostics and treatment application, it appeared during studies that the major drawback leading to unnecessary deaths is neither the shortage of drugs to treat nor shortage of equipment to diagnose, but the time taken to provide treatment to highly infected areas. The old modus operandi in health departments and diagnostics costs the country lives every year through delayed response to urgent fatal disease cases after diagnosis.

3.1 Bio conjugation and flocculation assay of AuNPs

The synthesized AuNPs were characterised using UV-Visible spectrophotometry and TEM, as shown in Fig. 3.1; The UV-Vis spectra show the results of flocculation assay using NaCl, which is very critical in demonstrating the stability of AuNPs before bio-conjugation. To determine color and concentration of the AuNPs, RGB values were used and solutions on of Fig. 3.2. To evaluate the critical stability and kinetics of AuNPs and bio-conjugates, BSA protein was used. It can be observed in Fig. 3.7A and B that the critical point of the stability of AuNPs was achieved with 35 mM NaCl (color of spectrum) concentration which is the point of intersection at the flocculation study. At this point, AuNPs form an aggregate which can be confirmed by the gradual change of unconjugated AuNPs from a red to maroon to purple colour upon addition of salt in a concentration from 10 to 50 mM as shown in Fig. 3.1A

and B. Further confirmation of this aggregation is clearly visible in the UV-Visible spectra of Fig. 3.1A, where there is a red-shift of the AuNPs surface Plasmon resonance peak from 525 nm to 640 ± 10 nm.

Fig. 3.1A, shows the uniform distribution of AuNPs with an average size of 14 nm also confirmed by Fig. 3.7A. After bio-conjugation of the particles with BSA, the 4 X diluted sample was scanned for absorbance in the wavelength range of 400 – 800 nm. Thereafter, additions of NaCl were made to check for the stability and effectiveness of conjugation. Interestingly, as shown in Fig. 3.1B, there was no colour change and the absorbance remained at 525 nm, therefore, 70 mM of NaCl confirmed that the bio conjugation of NPs can tolerate the amount of salt. This demonstrated the critical concentration of pLDH antibody which was added on the surface of AuNPs, a bioconjugate system that was used to fabricate the dual channel lateral flow kit for malaria.

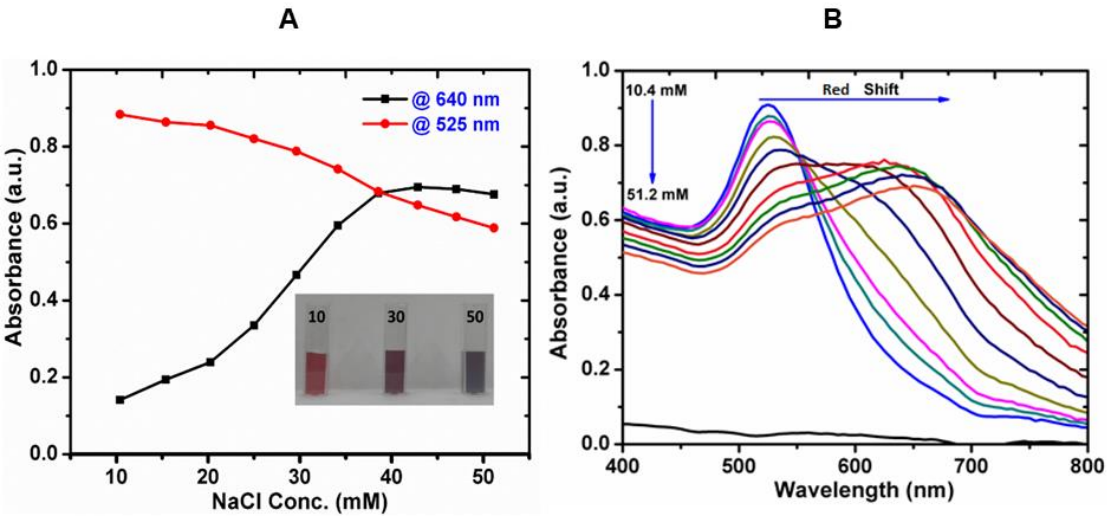

Figure 3.1: (A) Shows the UV scans for the flocculation study of AuNPs NaCl at concentrations from 10.4 to 51.2 mM. (B) A significant decrease in the absorption maxima for AuNPs is observed at 525 nm with the formation of new absorption band at 640 nm

3.2 Optimization of Salt content

A flocculation study was performed on AuNPs with NaCl concentration range of (10. 4 mM – 51. 2 mM). The study was performed to investigate the stability of AuNPs on NaCl before bio-conjugation with BSA which helped comprehend impact of salty blood samples on lateral flow efficiency. The concentration, at which optimum absorption of AuNPs-NaCl was achieved, was marked as the highest concentration of suppressant tolerable by test kit. The decrease in absorption maxima at 525 nm confirmed NaCl as suppressant, with an increase in absorption maxima at 640 nm occurred through addition of salt from 10.4 – the highest formation peak at 51.2 mM salt where the absorption due to salt suppressant stopped forming a new upper peak at 640 nm. The conjugation study as depicted in Fig. 3.1A shows a graphical trend in the UV visible spectrum where at 525 nm, AuNPs absorb UV light and forms a sharp absorption band with no other absorption. Addition of salt particularly 10,4 mM NaCl in the bare – AuNPs decreased maximum absorption at 525 while forming a new absorption band at 640 nm due to NaCl suppressing signal. As the concentration of NaCl increased, there was an inverse proportion relationship observed in the spectrum between initial absorption and new formation absorption band. A reaction kinetics interpretation of Fig. 3.1A is shown in Fig. 3.1B where at 0 mM NaCl, the reactants (red graph) were at 100% absorption, 0% products (black graph), after addition of 10.1 mM and waited for 20 seconds, a decrease on reactants was observed with growth on product side up to the equivalence point where the amount of products is equal to the reactants. The continuation of the study led to a discovery of the highest concentration of salt corresponding to maximum products and depletion of reactants at 51.2 mM.

3.3 RGB Value Colour of Gold Nanoparticles

Gold nanoparticles stabilized with citrate have a maroon colour, while Gold nanoparticle with citrate and NaCl show a somewhat dark purple colour due to reaction of NaCl which demonstrate the instability of citrate gold nanoparticles. However, upon bioconjugating with antibodies they resist any effect of the salt,

thus, remaining stable. These test as discussed above are used to distinguish between conjugated and unconjugated gold nanoparticles. The colour change during flocculation is not easily detected with our eyes. We have therefore used RGB values to demonstrate this effect. RGB is an acronym for Red, Green and Blue. The software uses all three colours to determine the colour on a picture through subtraction on the spectrum. The pictures were taken using a Samsung J1-ACE with 5 mega pixel camera.

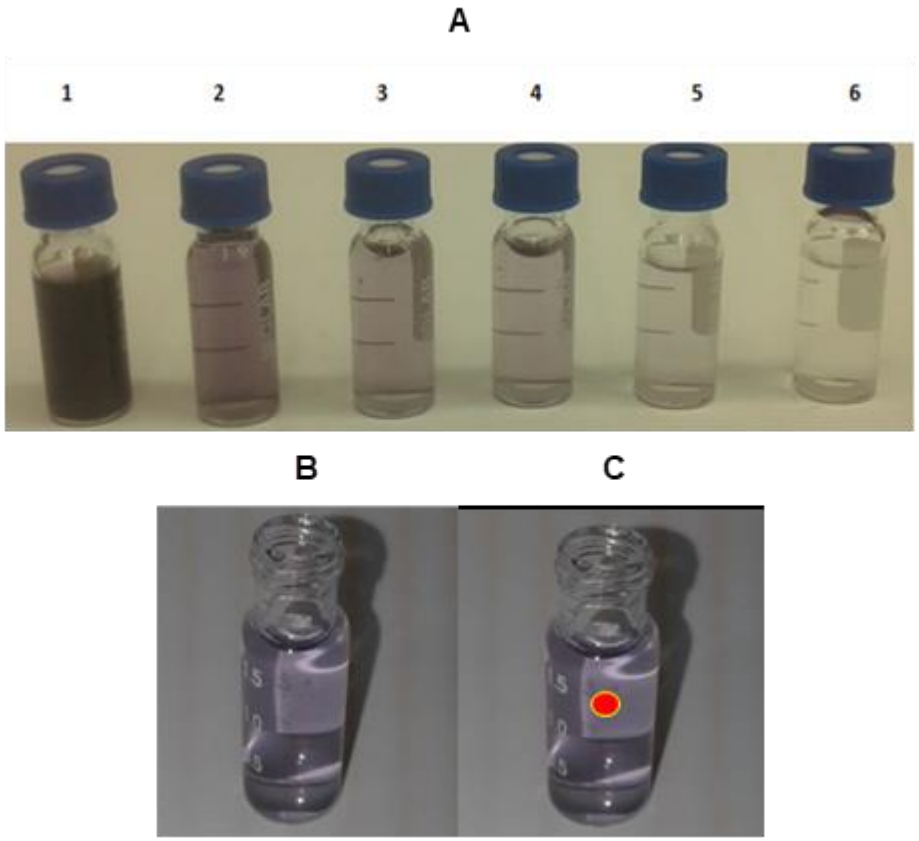

Figure 3.2: Pictures of AuNPs at different metal concentrations stabilized with sodium citrate. (A) 1 – 6 (1, 0.8, 0.6, 0.4 & 0.2 $mg.L^{-1}$) respectively. 0 $mg.L^{-1}$ contains water as a blank at number 6. (B) 0.4 mg. L^{-1} concentration clear picture to be uploaded for analysis, (C) A 0.4 $mg.L^{-1}$ AuNPs with a RGB spot marked.

Table 3.1: Red, Green and Blue values determination in quantification.

Picture	NaCl Concentration ($mg.L^{-1}$)	Red	Green	Blue	HTML code	HSV code	Volume (mL)
6	0	108	108	108	#161618	240° 8.33% 9.41%	1
5	0,2	87	86	91	#25222D	256.36° 24.44% 17.65%	1
4	0,4	73	63	74	#312E34	270° 11.54% 20.39%	1
3	0,6	49	46	52	#493F4A	294.55° 14.86% 29.02%	1
2	0,8	37	34	45	#57565B	252° 5.49% 35.69%	1
1	1	22	22	24	#6C6C6C	0° 0% 42.35%	1

The codes generated are unique to a specific colour uploaded and analysed by the RGB generator and their accuracy depends image quality.

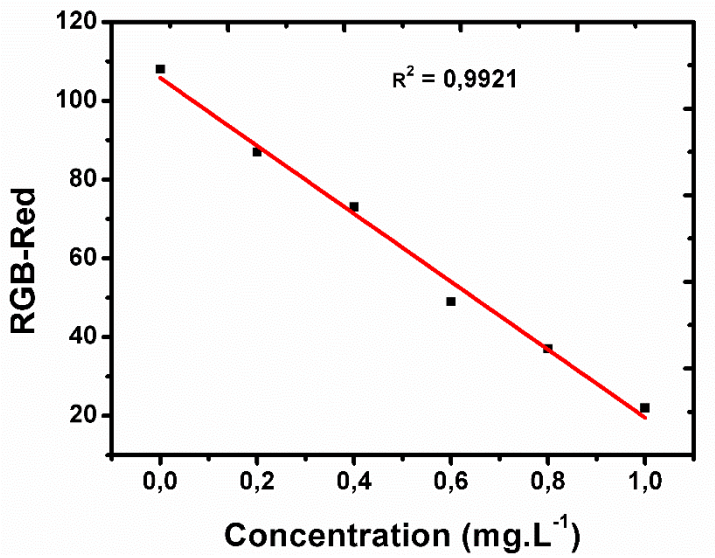

Figure 3.3: The graph shows the first point is water, sodium chloride 0.2, 0.4, 0.6, 0.8, and 1 $mg.L^{-1}$ AuNPs. The correlation co-efficient is 0.9921 which is close to 1. RGB – Red value plotted against concentration.

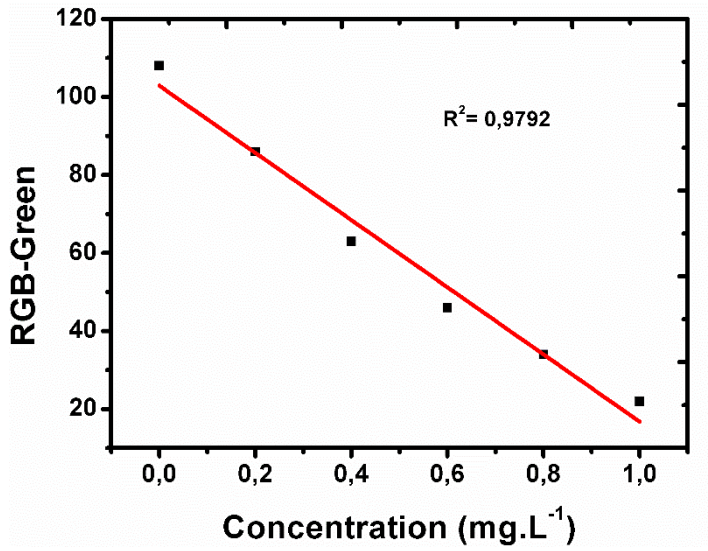

Figure 3.4: RGB - Green value plotted against concentration of solution. The behaviour of Green in a straight line is not good as the co – relation co-efficient is 0.9792 not so close to the reference value 1.

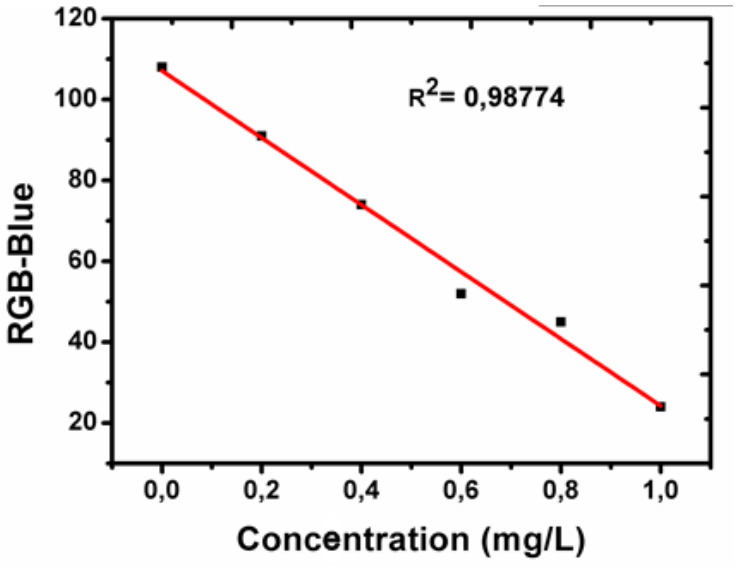

Figure 3.5: RGB - Blue value plotted against concentration of solution. The behaviour of blue in a straight line is good as the correlation co-efficient is 0.9902 n close to the reference value 1.

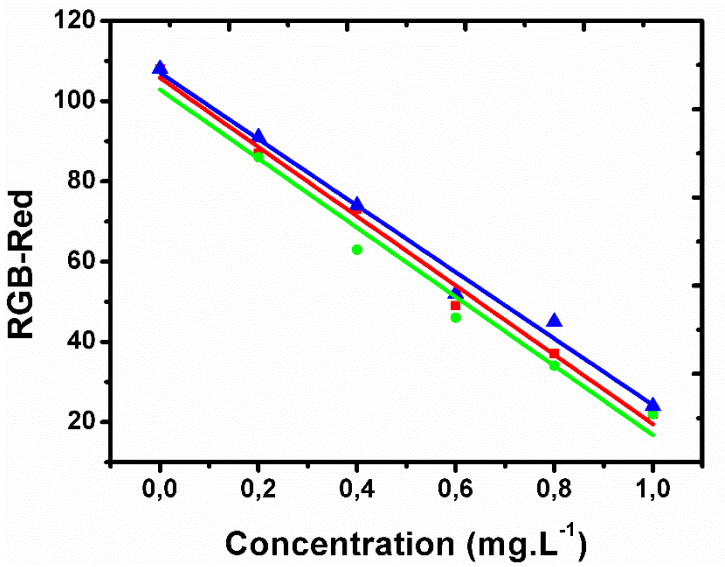

Figure 3.6: RGB values plotted against concentration of solution. The behaviour of all three lines somewhat cluttered with red being better since the colour of the AuNPs is slightly reddish.

The RGB values have been used to plot a graph of RGB against concentration of NaCl. The nanoparticles used had NaCl in the range of 0.2, 0.4, 0.6, 0.8 and 1 $mg.L^{-1}$ and all have different colors. The solution of AuNPs with the highest salt concentration appeared darker whiles the least lighter. The

Red graph shows red as a more accurately detected color in the picture taken with a cell phone of 3 MP camera. Red linear curve had R^2 of 0.9921 which deviated by 0.0079 units from the standard accuracy of a best straight line. The Green color gave R^2 value of 0.9792 which is not a good representation of an accurate straight line graph to depict a linear relationship, the green is 0.0208 away from the standard 1 of superior accuracy of straight line. While blue showed a better correlation co-efficient R^2 value, it was also not better than Red in accuracy of RGB points forming a straight line. Blue had R^2 0.9902 and had 0.0098 deviation from 1. The color of the analysed samples is purple to dark blue which made blue the most absorbed color, green less absorbed and red as a reference, the most. Green was the least detected color in the spectrum. The graph on Fig. 3.6 is a combination of all three color line graphs in the intension to establish a relationship between RGB of AuNPs and concentration of salt. This sample can be quantified for red colored samples using the most accurate graph. The same volume of 1 mL per concentration was used and same containers. As indicated in Fig. 3.3 – 3.5, as the concentration of NaCl increased, RGB value decreased which denoted a relationship between the two variables. RGB value of AuNPs is inversely proportional to concentration of NaCl. RGB α NaCl concentration ($mg.L^{-1}$).

3.4 Optimization of Antibody Concentrations and Detection of Malaria

When a sample containing recombinant pLDH (Ag) was passed through the test strip, two pinkish red lines were observed. The principle of a working kit is shown in Fig. 2.2 in which the sample pad is separated from the conjugate pad by inserting a plastic barrier between the two sample pads which prevent any contact of the analyte sample before reaching the test line. This assay is referred to as the dual channel because the sample is allowed to reach test line, unlike normal lateral flow where the sample and conjugate are allowed to arrive at the test line simultaneously. The appearance of only the control line may be due to the absence of detectable antigens in the sample to form an analyte-detector complex.

In Fig. 2.2, when a blank sample containing no pLDH (Ag) was passed through the test strip, one pink line (control line) was observed which was due to colloidal AuNPs-anti-pLDH (primary Ab) reacting with the anti-mouse IgG (secondary Ab). These formats clearly distinguished positive and negative samples, as shown in Fig. 2.2, where only the control line is observed when there is no reaction between the antigen and antibody.

3.5 Transmission Electron Microscopy and UV-Visible Studies of AuNPs with protein BSA

The transmission electron microscopy (TEM) also sometimes conventional transmission electron microscopy (CTEM) is a microscopy technique which transmit a beam of electrons through a specimen (mostly ultrathin section less than 100 nm thick or a suspension on a grid) to form an image thrugh the interaction of electrons and with the sample as the beam is transmitted through the specimen. A TEM instrument is capable of imaging at a significantly higher resolution than light microscope due to a smaller deBroglie wavelength of electrons.

$$ƛ = \frac{h}{p} \qquad (2)$$

Where h is the plank constant, p is the momentum of the particle and ƛ is the deBroglie wavelength.

The data generated on Table 3.2 was aimed at studying and understanding the behaviour of AuNPs in a blood sample, leading to the best concentration choice of BSA and AuNPs for the establishment of the best flocculation for capillary action. Fig. 3.7B shows the absorbance increases with a direct increase in concentration of protein and bio conjugated AuNPs at the same constant wavelength

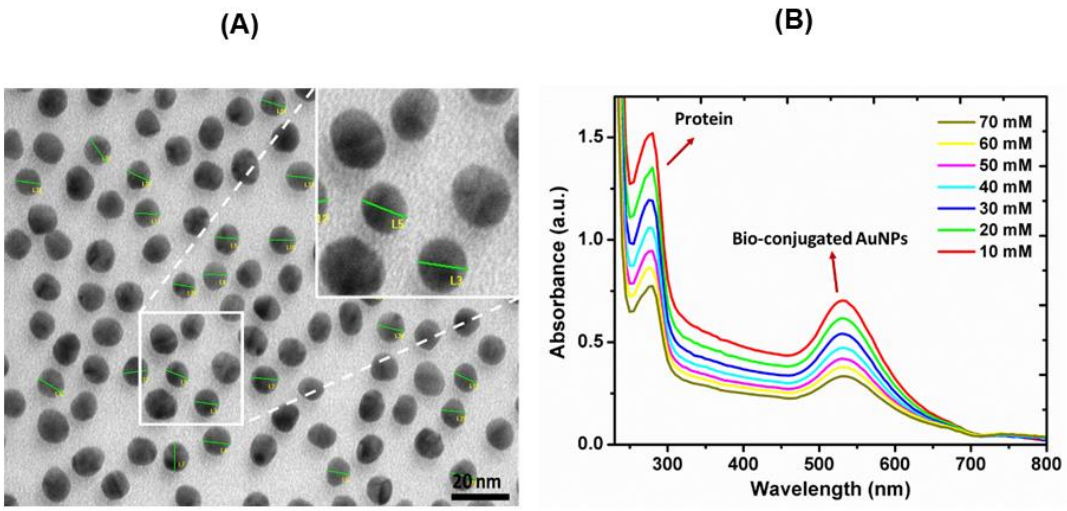

Figure 3.7: (A) Flocculation study showing stability of the conjugated nanoparticles in a NaCl range 10 to 70 mM. (B) Morphology of evenly distributed bioconjugated nanoparticles with average size of 14 nm. Insert confirm particle size distribution.

Table 3.2: UV-Visible absorption bands of AuNPs at different concentrations of BSA protein.

Wavelength (nm)	Absorbance	Concentration (mM)
279,989502	0,763879716	10
279,989502	0,84755224	20
279,989502	0,945509672	30
279,989502	1,063843608	40
279,989502	1,208243012	50
279,989502	1,373480201	60
279,989502	1,581143975	70

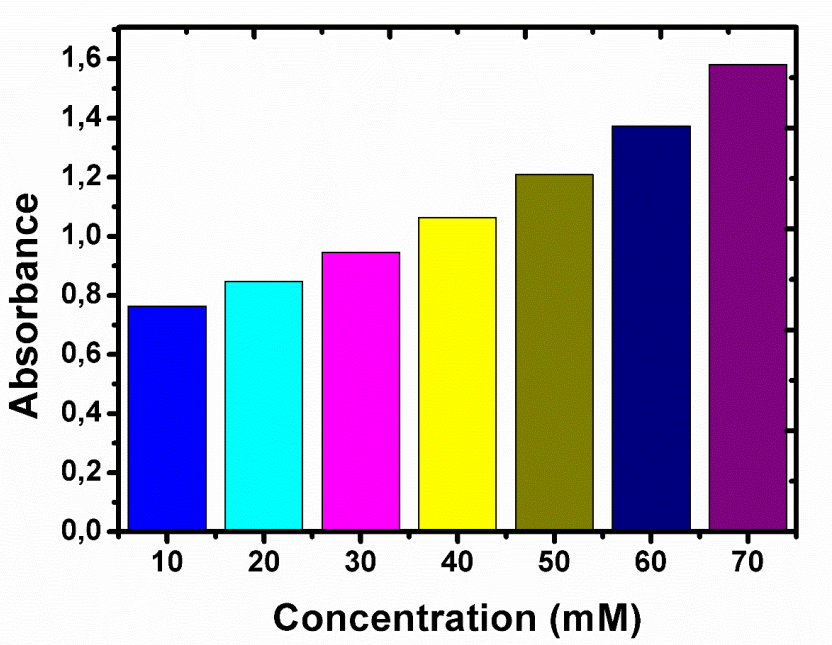

Figure 3.8: A bar graph representation of addition of protein on gold nanoparticles with different salt concentrations.

3.6 Semi-quantitative assay using line intensity

A variety of concentrations from 10, 50, 100, 200 and 300 ng.mL^{-1} samples of pLDH were tested on the prepared lateral flow. The test line was immobilized with anti-pLDH which reacted with pLHD antibodies from the sample introduced on sample pad. The control line was also immobilized on concentration range as above to examine the line intensities.

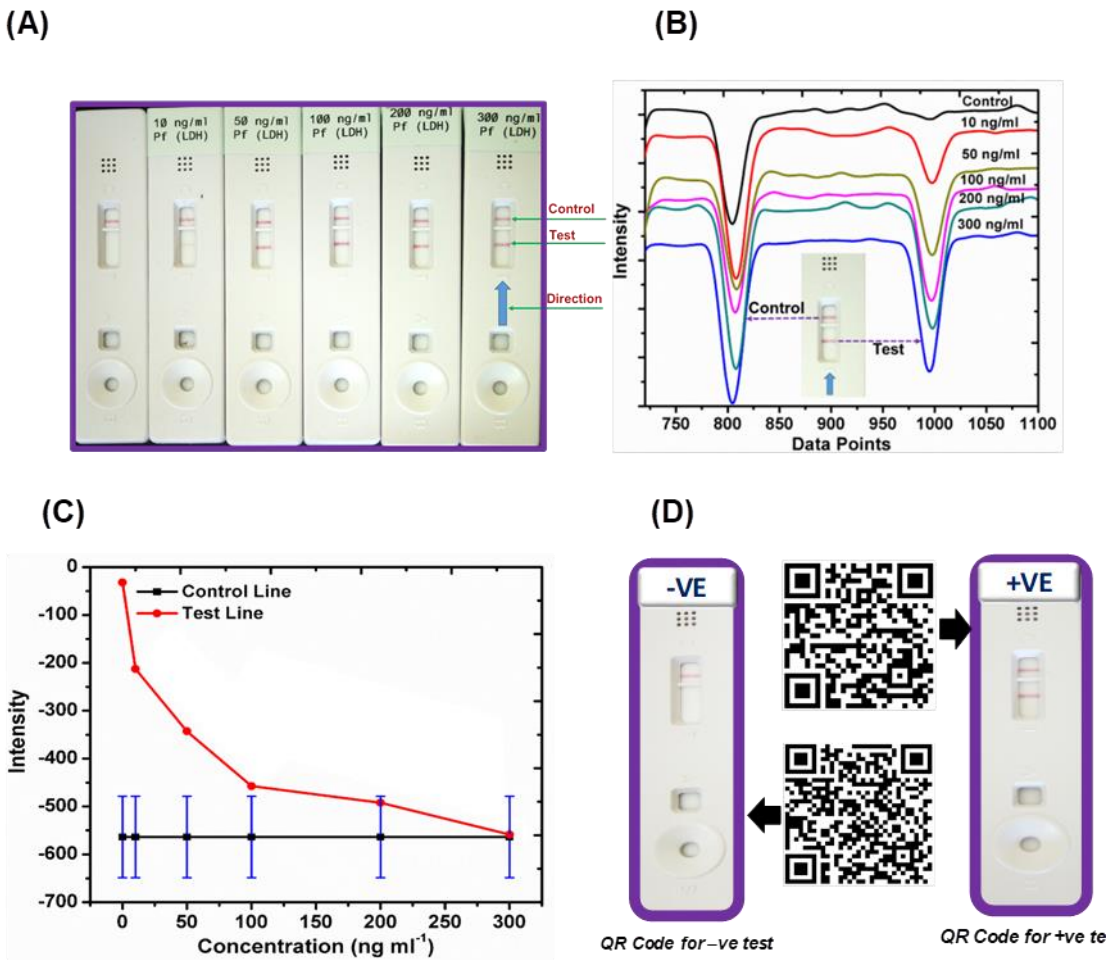

Figure 3.9: Rapid test kit with 10 – 300 ng.mL^{-1} pLDH, the first left kit is a negative far right pLDH highest concentration examined showing. Increase in colour intensity as concentration increases. (A) Showing an image of the test strip on fixed data point with varying concentration. (B) An increase in the intensity of the line is observed from 10 to 300 ng ml^{-1} with increasing concentration (C) Plot of intensity of control and test lines againt concentration. (D) Unmodified QR barcodes for positive and negative tests.

Fig. 3.9B represents the data obtained from the ESI quanti-colorimetric intensity reader for both test and control lines observable in the test kit shown in Fig. 3.9A. The graphical representation of test strip line intensities for both control and test lines in Fig. 3.9B is approximately at 800 and 1000 data points, respectively, on the x-axis of the graph. The results of the intensity reading are in agreement with the concentration of the analyte. The trend can clearly be observed going from 10 to 300 ng.mL^{-1}, with the intensity gradually increasing depending on the concentration of the analyte. The test line intensity mainly

arises from the concentration of the AuNPs bioconjugate which reaches the secondary antibody immobilized on the control line. The result form the intensity reader can be used to develop a semi-quantitative lateral flow assay; this can easily be demonstrated by plotting a straight line of the concentration and the intensity which correspond to each spiked antigen. Thus, to obtain semi-quantification results, an intensity reader; thus, its concentration can be extrapolated from the linear region of the graph.

Accordingly, the intensity reader can be used to determine the extent of infection by considering primary and secondary immune responses. The developed dual lateral flow immunoassay showed high sensitivity adding to its many advantages, going down to nano-scale in its Plasmodium detection ability. The sensitivity of the rapid diagnostic test significantly of the malaria parasite; hence, there is a direct correlation between the analyte concentration and intensity of the test line as shown in Fig. 3.9C. A series of concentrations prepared from as low as $ng.mL^{-1}$ were tested on the lateral flow kit and positive result was observed for the lowest with faint line, making kits highly sensitive. The same samples were repeated on the control signal, the line is satisfactorily visible to distinguish the test samples as either positive or negative depending on the availability of the test line. Interestingly, the lowest bare eye detectable concentration was found to be 10 $ng.mL^{-1}$, while the calibration plot showed two linear parts with a regression co-efficient of 0.9793 in the range of 10 to 100 ng mL^{-1} (part I) and 0.9373 in the range of 100 to 300 $ng.mL^{-1}$ (part II). Based on the intensity, it is accurate judgement to conclude that the lower detection range was the best as there was a more intense signal observed.

3.7 Fabrication of QR codes, two and three coded

The fabrication of QR codes occurred in the dual and tri-coded system. Overlaying of QR codes is detailed in each section.

3.8 Two Dimensional QR codes

Two dimensional QR code sequencing, optimization and application is achieved through accurate decoding top left of two QR codes, right angle positioning and overlaying. This design comprises of the positive and the negative code, invalid is assumed when a case of no control binding occurs. There is no scanning required where invalid is observed making this design a scanning only on bare eye observation of positive and negative as shown on Fig. 3.10 below.

Figure 3.10: Two QR code design with positive and negative codes overlaid accurately.

To scan QR codes, a Samsung J1-Ace built with 1.2 GHz quad core processor, 5 mega pixels AF + 2MP camera was used.

3.9 Three Dimensional QR Codes

The three QR design provides a more complex system of diagnosing and tracking malaria using the QR code technique. In this design, three QR codes and decoded, positioned at right angles corner face and overlaid, where the first top is a positive, centre being negative, bottom last as an invalid test and all

cases are traceable in this test design. The three QR code design constitutes of three de-coding boxes for test, control and invalid lines as shown on Fig. 3.11, all three codes are at 90 degree angle of overlay.

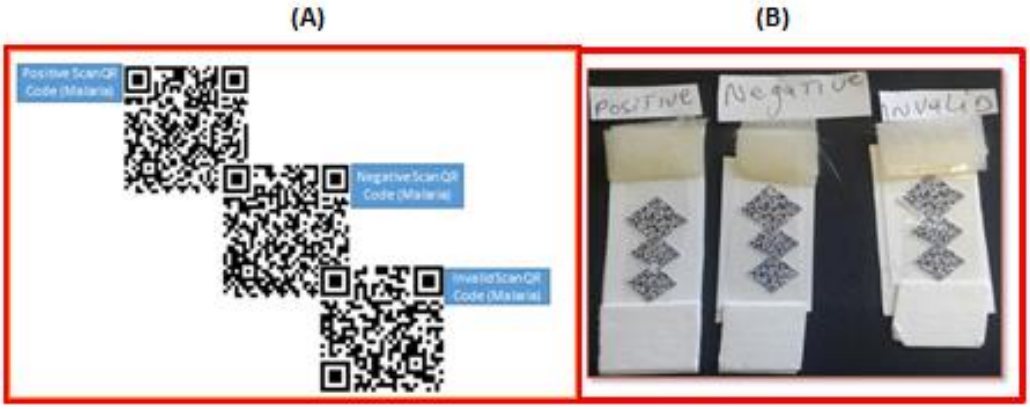

Figure 3.11: Three codes at 90 degrees overlay with positive, negative and an invalid test. (A) The overlaid QR codes for a 3D Barcode lateral flow, (B) A real image of a 3D barcode based lateral flow concept design.

3.10 Real time data capture with QR code

The principle of a novel design for collecting and storing information involves the use of QR code application that is freely available for smartphones or any other compatible gadget. This approach enables rapid global tracking and storing a lot of data for positive and negative results during malaria analysis; therefore, respective QR codes are assigned as shown in Fig. 3.12D. The QR code has been compressed to fit in a normal test kit size and no more than the usually applied quantity of the antibody/antigen or AuNPs is required as shown in Fig. 3.12C & D. The design of the QR code is generated for all possible testing results and linked to Google Analytics. Firstly, the QR code is encoded with a website linking it to positive or any other possibilities. Then, the script is embedded into the website which is linked to Google Analytics. This enables data to be collected each time a user scans the specific QR codes. Upon the scanning of this QR code, there is a lot of data that can be obtained from a single scan such as the geological position of the scanned lateral flow assay as

well as to distinguish whether the results are positive or not, and even the information on the device that was used can also be obtained.

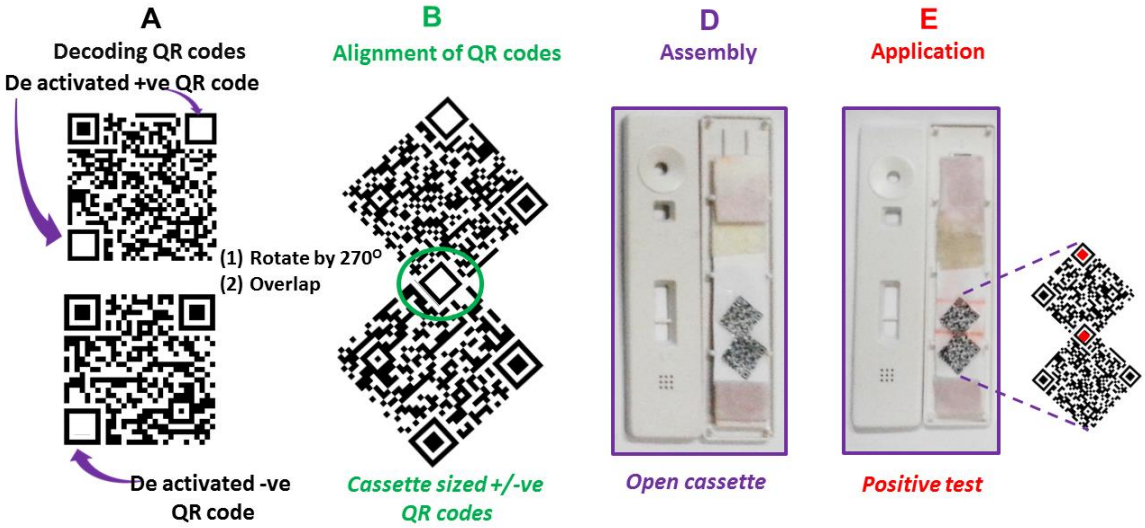

Figure 3.12: Stepwise procedure for the modification of QR barcodes for installation and application using test as an example.

The codes generated with the QR codes generator online software were modified specifically for application on the lateral flow technology by deactivating them as depicted in Fig. 3.13, where the centre squares in the corners of the QR code are removed. Under this circumstance, all scans are invalid as the codes are deactivated. However, when there is an antibody placed for binding, the red colour replaces the missing part of the QR code; hence, the test line activates the QR code. The first line (top) will activate the code corresponding to the positive test, while the second line activates the one for control line as shown in Fig. 3.13A. This system is designed to accommodate three possibilities: positive, negative and invalid results as depicted in Fig. 3.13A.

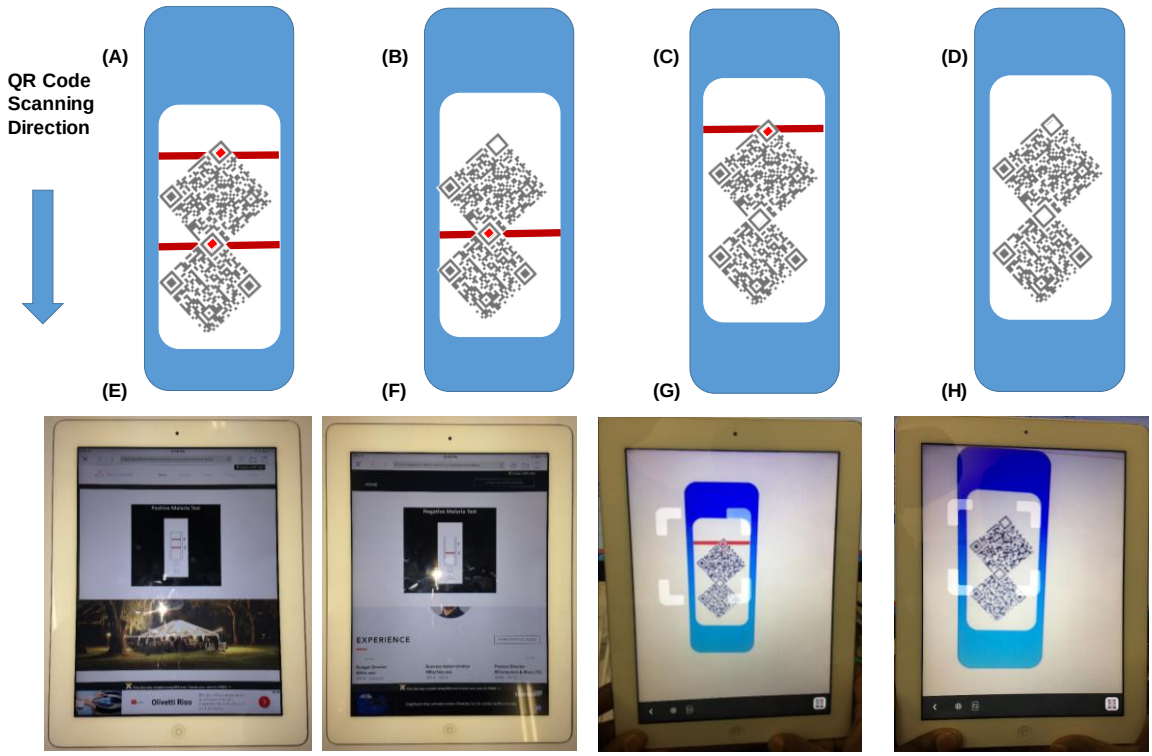

Figure 3.13: Two QR code system design and overlaying. (A) a positive design of QR code embedded lateral flow, (B) a negative scenario, (C) is an invalid test with only test line and no control, (D) no line observed represents an invalid test design, (E) is a positive website design, (F) a negative website design, (G) an invalid website with test line only, (H) an invalid website design without lines.

An important part of the study that brings a unique technology not available anywhere is the QR barcode and the way Google Analytics has been applied to the testing kits. Data analysis and tracking render the developed testing kit an incredible technology advancement in the diagnostics industry, after the sample has reached the sample pad a scan utilizing a cell phone camera through a QR code software, automatically direct the user to a wix website that is well developed and modified to identify results. The website has codes embedded in it to enable results tracking and statistical data capture of all users of the testing kit. Demographics are provided in the Google analytics tracking tool down to location specific. The tracking tool provides also real-time information of number of users, their specific location and results of the test, negative, positive or an invalid test.

3.11 Graphical Representation of line intensities

Line intensities are important to be accurately studied in lateral flow since they are the sole representation of antigen and antibody binding efficiency. The study of line intensities minimizes errors in bare – eye detection lateral flow immune-assays through revealing deficiencies in antibody and assisting in determination of the optimal antigen required for an accurate diagnosis of even the lowest antibody. It is important in lateral flow to optimize the amount of reagents use to minimize false results or indecisive results. The data below presents line intensities in a graphical system to understand the trend and realise optimal values. Fig. 3.9B contains data on line intensities and that has been populated graphical and table form.

Table 3.3: Data for the study of control line intensity using Quanti Reader

Wavelength (nm)	Concentration (ng.mL-1)	Intensity
740,8727	10	610,9214
740,8727	50	680,9741
740,8727	100	737,2324
740,8727	200	798,9511
740,8727	300	938,6042

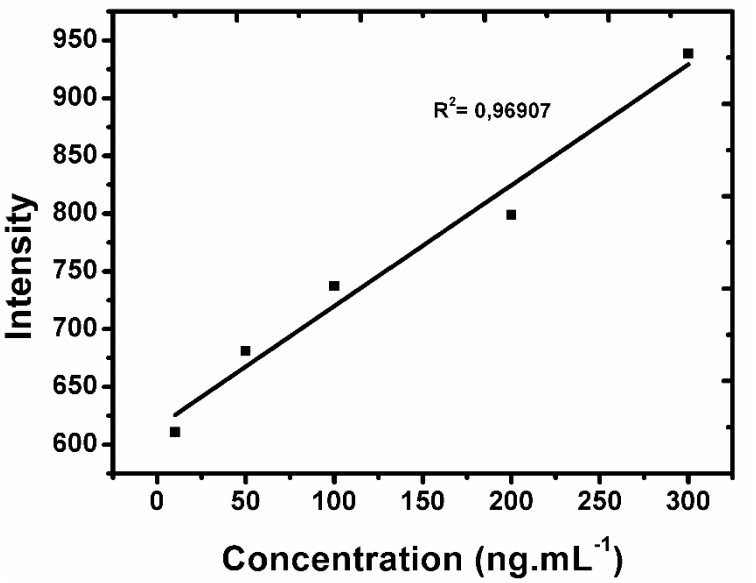

Figure 3.14: The line graph of intensity Vs concentration of Antigen on the testing kit, the graph shows an observable direct proportionality between intensity and concentration using a Quanti reader.

The intensity of red control line on the testing kit examined on a range of concentration where a universal antibody was used binding with the primary antibody immobilized on AuNPs. The increase in concentration of the control antibody is explained in Fig. 3.9 which increases the intensity of the control line, there is a direct proportion relationship observed between antibody concentration and line intensity. The trend shown in Fig. 3.9A, as concentration of antigen increases the clearer and strong a test line is.

Table 3.4: Data for the study of test line intensity using Quanti Reader

Wavelength (nm)	Concentration (ng.mL-1)	Intensity
856,9468	10	800,5729
856,9468	50	855,5403
856,9468	100	992,6594
856,9468	200	1254,147
856,9468	300	1327,366

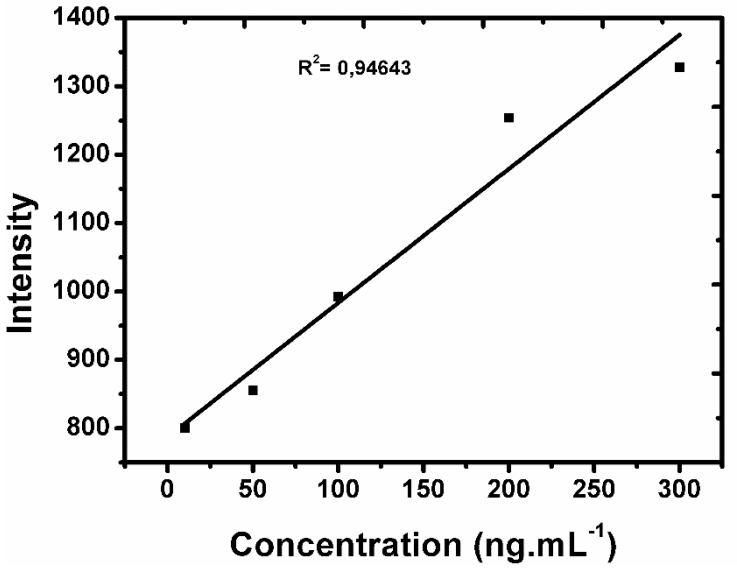

Figure 3.15: Graph generated on study of line intensity reported on Fig. 3.9B. The test line shows a low intensity on 10 ng/mL and high intensity at 300 ng.mL^{-1}.

As the antigen concentration increases, the intensity of the test line as observed on the graph and on Fig. 3.9A increases. A faint line corresponds to a low antigen concentration on blood taken from patient.

3.12 Scanning Distance and Response

The scanning distance is vital section of the developed technological immunoassay; a proper measurement is established detailing the optimum distance (see *Table 3.5)* for accurate numbers. The time it takes to capture is hypothetically dependent on optimal distance between the camera eye and overlaid QR barcode.

Table 3.5: Optimization of Modified QR Code Scanning distance and efficiency

Scan No	Scan type	Distance (mm)	Response time (s)
1	Positive	150	2
2	Positive	152	3
3	Positive	152	3
4	Positive	150	2
5	Negative	148	2
6	Negative	148	2
7	Negative	148	2
8	Negative	147	1
9	Invalid	150	1
10	Invalid	152	2
11	Invalid	152	2
12	Invalid	152	2
Calculation	Average	150,08	2

3.13 Distance optimization between Camera eye and QR code

The distance study involved accurate measurement of the smart phone distance away from the angle overlaid codes and the recorded measurements in Table 3.5 were taken where the QR code software achieved a result website link.

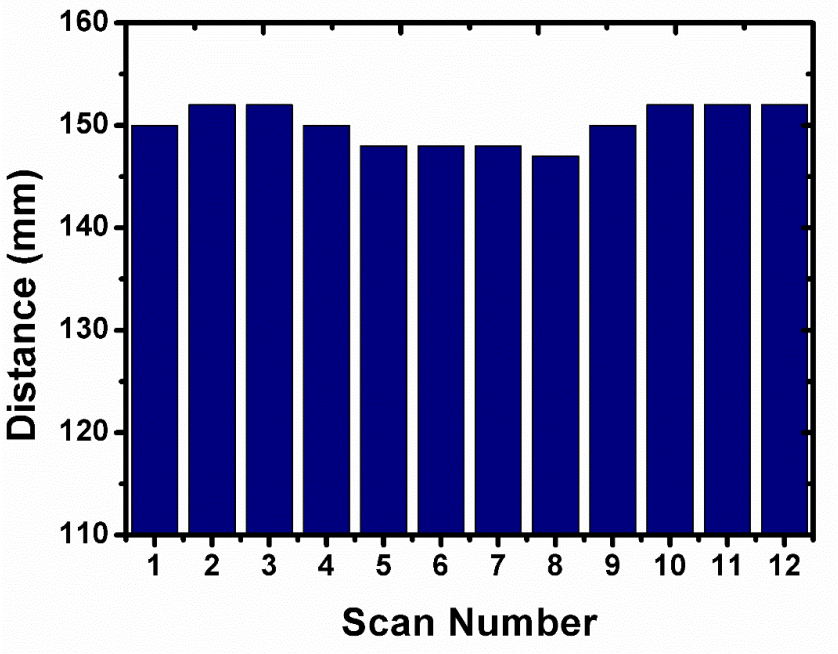

Figure 3.16: Scanner distance optimization study. Repetitions of 3 groups of possibilities of the test results, where positive (1 – 4) bar, negative (5 – 8) and invalid (9 – 12) bar give a mean optimum distance.

3.14 Optimal distance response time

The optimal distance study lead to a time study to evaluate how long it takes the camera at the optimized distance to record a signal corresponding to accurate results and Table 3.5 consist of data for the plot. The distance where the scanner should be to accurately pick up QR code sequence and deduce results is optimized below.

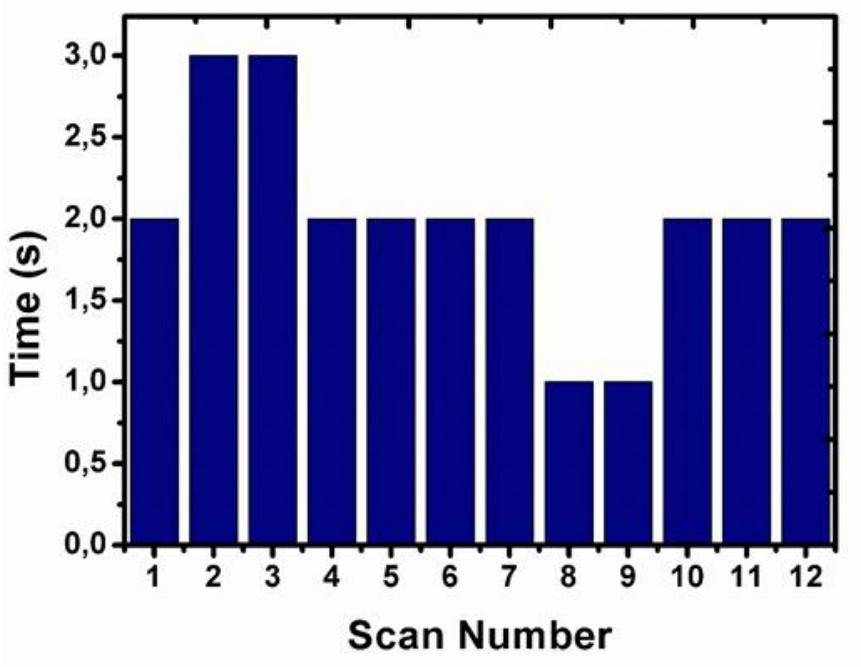

Figure 3.17: A measurement of time (s) duration the 5MP AF camera takes to record/capture a website link result on overlaid QR barcode sequence. The average is taken.

3.15 Assembling and testing using QR code test kits

After the sample has fully migrated in the sample pad and through the entire test kit, a QR scan is then performed which reflects the results on Google Analytics, where real-time data either positive or negative accordingly is tracked and observed. The tracker provides specific information such as continent, country; city, area and time at which the scan was performed as on Fig. 3.18C. It is interesting to note that the QR code and Google Analytics tracker of the website were successfully utilized for the first time in a lateral flow assay. In addition, valuable information on either positive or negative results was also encoded for the analyst to go through after performing the test depending on the outcome of the test. Google Analytics enables test monitoring in all countries across the globe as shown in Fig. 3.18C**.** Detailed information on the Geographical location of the users, namely city, village, or township/suburb, can also be successfully extracted from Google Analytics as depicted on Fig. 3.18C. This study took a step further looking at the browsers used, where it was

observed that Google Chrome was the most utilized with 77.45% sessions, followed by Edge at 13.73% sessions and Safari at 7.84% sessions. More data is available to as far as the time of the scan and the type of operating system.

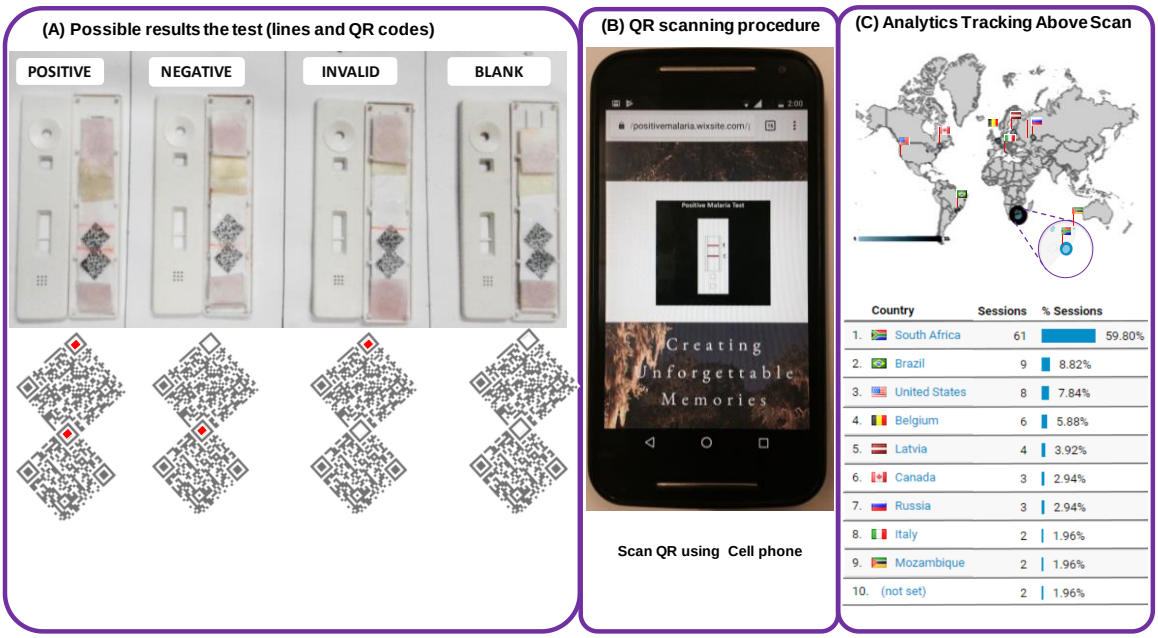

Figure 3.18: QR code generated for the invalid scan with the corresponding lateral flow image representing positive, negative, and invalid tests. (B) Shows the order from the QR barcode to Google Analytics. A cell phone with the QR code application or a QR code scanner scans the test kit which uses an internet connection to link the website with simultaneous tracking on Google Analytics. (C) Statistical Google Analytics data with real-time monitoring of number of users, location, duration, results (positive, negative or invalid) etc. Graphical representation of data points tracking usage of the test kit, website and QR code.

We believe that the information provided on Fig. 3.18 could be very useful in the surveillance study of the actual disease while providing real-time measurements. These scans could provide very important information especially with regards to the system used at point-of-care to capture results; it could be seen that the type of operating system is also captured by Google Analytics which makes the method even more detailed and specific in terms of identifying each test user.

The information in the Table 3.6 below represents all the countries that participated in the trial and testing of Malaria Plasmodium Lactate – dehydrogenase using the newly developed QR based testing kit. A total of 100 sessions were recorded in all the countries grouped together and South Africa has the highest number 61 sessions since the study was first developed and tested in various areas of KwaZulu Natal, Durban.

Table 3.6: Countries that tested the QR based lateral flow

COUNTRY		SESSIONS	% Sessions
South Africa	SA	61	59,8
Brazil	Br	9	8,82
United State	US	8	7,84
Belgium	Be	6	5,88
latvia	Lat	4	3,92
Canada	Can	3	2,94
Russia	Rus	3	2,94
Italy	Ita	2	1,96
Mozambique	Moz	2	1,96
Not SET	NS	2	1,96
		100	98,02

A Google Analytics tabulation of Geographic information on tests performed**.** The information tabulated is an elaboration of Fig. 3.18C, which is a Google Analytics raw data and Geographic location as per website, tracking and statistics. There were total positive scans of 59.8% in South Africa, followed by Brazil at 8.82 %, (9 sessions), the United States at 7.84% (8 sessions), Belgium at 5.88% (6 sessions), Latvia at 3.92% (4 sessions), Italy and Mozambique at 1.96% (2 sessions).

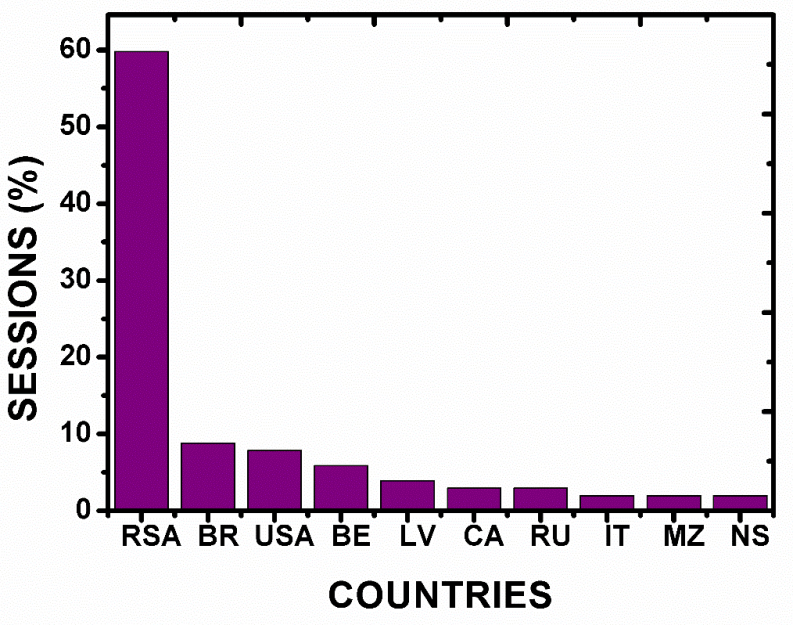

Figure 3.19: Graphical representation of countries that tested the QR based testing kit and sessions of test. South Africa showed as the country with highest users and Mozambique the lowest.

More countries could still be contacted for scans and increase the number and percentage scans; however, the study has enough data points according to proof of concept and has demonstrated beyond scientific data that the concept brings a genuine approach to the diagnostics. The above graph on Fig. 3.19 and Table 3.6 show a decreasing trend in sessions that happened in different countries from the highest which is South Africa, to the lowest which is Mozambique and Italy.

3.16 Monitoring of Browser Utilized

The website browsers that were used in the study are also captured on the Google Analytics tracking system; and with different countries come different browsers as tabulated on Table 3.7 and also graphically presented on Fig. 3.20. The most commonly utilized search engine internationally is Google and it offers upgrade version and more services yearly. Google chrome appears as the highest utilized website browser when scans were performed as it is at 77.45%

sessions followed by Edge at 13.73% sessions, then Safari at around 7,84% and the last observed is Android Browser at 0.98% sessions.

Table 3.7: Website browsers used to read the results

WEBBROWSERS	% SESSIONS
Android Browser	0,98
Chrome	77,45
Safari	7,84
Edge	13,73

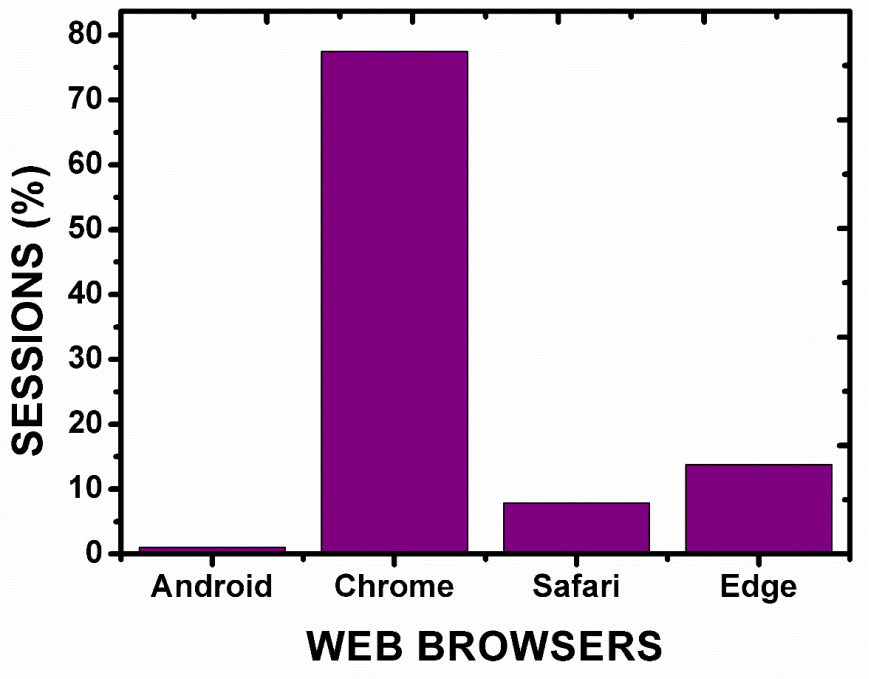

Figure 3.20: Graphical representation of website browsers used to read results, on all countries grouped. Chrome appears as the most used and as the Android least used search engine/device.

3.17 Statistical Data Analysis

The analysis of data from Google Analytics and QR code embedded rapid test kit is made convenient by the digitization of the system. Google Analytics has made it simpler to track all test results and report simultaneously. Fig. 3.21 depicts the website linking of QR codes and Google Analytics tracking of malaria personalized websites.

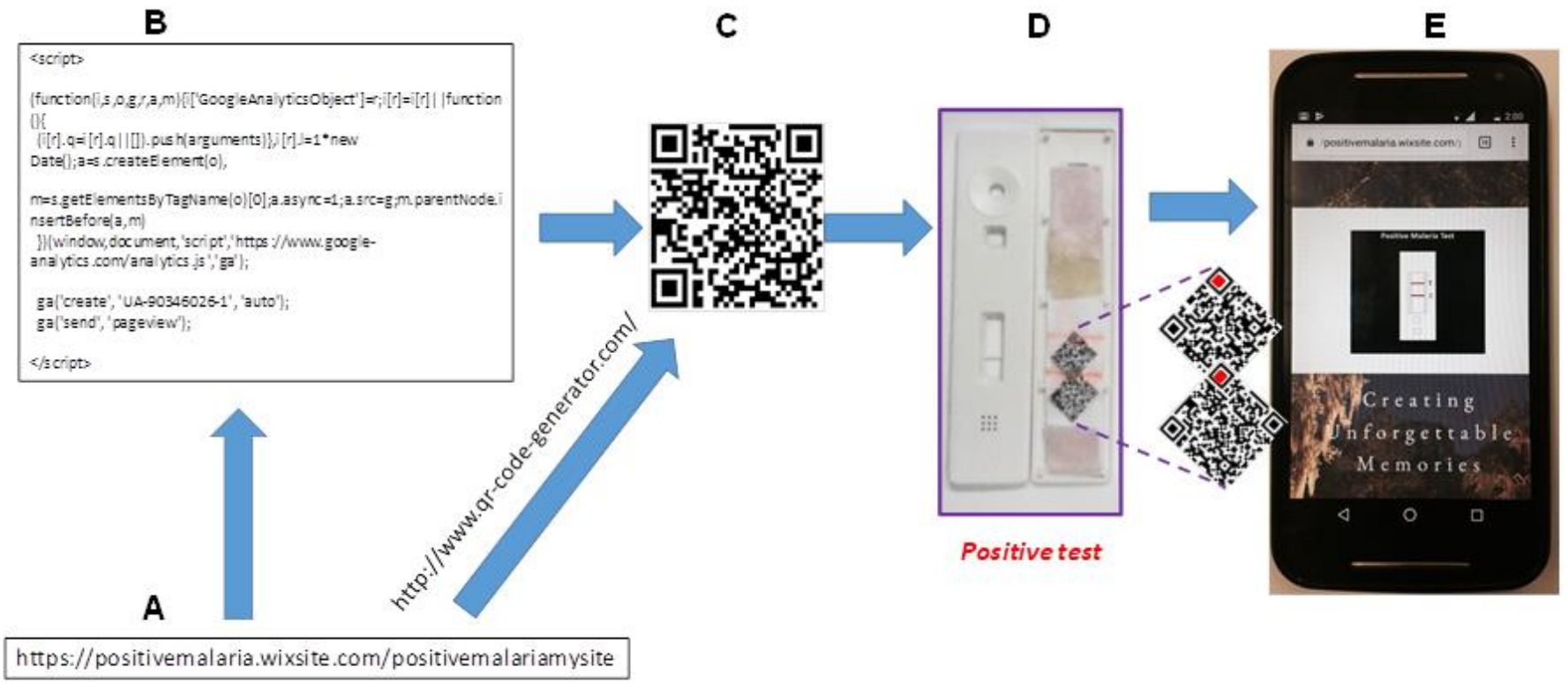

Figure 3.21: Design of Google analytics system from website where (A) Website designed using free online Wix (B) The Google analytics script used to link website to Google analytics (C) QR code designed using online QR code generator, (D) Lateral flow immune Assay and I Website after scanning QR code.

3.18 Linking of Wix Website with Google Analytics

The created wix websites have a back end of the site where editing and customisation happens, by logging in on wix website, it opens to the home page where domain and address are seen. Fig. 3.22 simplifies the whole concept of the newly designed website using a schematic diagram with arrows as seen above. First, an email is required to create an identifiable website (which was created) using Wix website creator. The emails created on Google, Gmail is positive@gmail.com, second; negative@gmail.com and invalid@gmail.com. The emails were each separately used to create a positive, negative and invalid websites on Wix. Then to link the website with Google Analytics, follow the steps below:

- On the home page of the website site, go to ‘’manage site’’, settings will appear.

- On settings page, go to ‘’edit site’’ button, the website editor tab will open

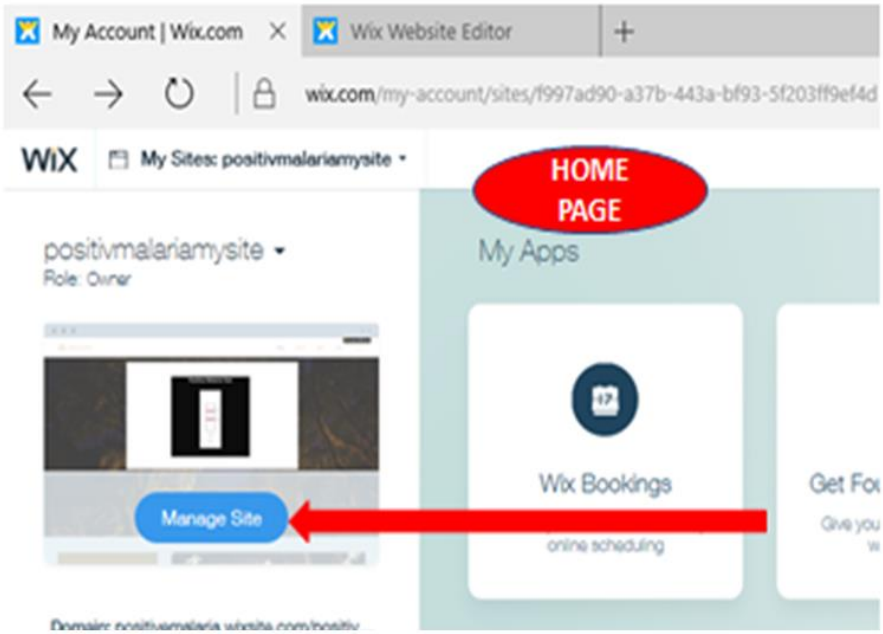

Figure 3.22: This shows the home page of the Wix website that is opened to track positive results. A snapshot from our page was taken.

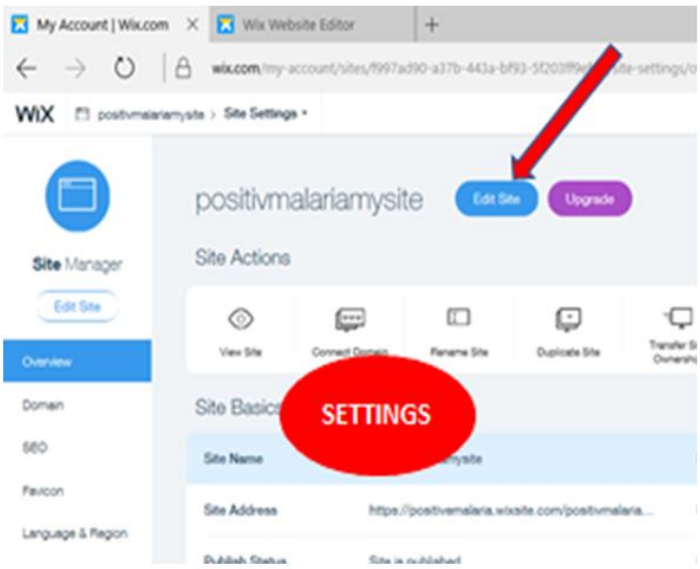

Figure 3.23: Shows the settings screen on a Wix website where that allows the website to be edited and customized to be able to link it with QR code system.

- On the website editor tab, left icons, go to ‘’ADD image’’, then upload an image relevant to the type of test being created i.e positive, negative or invalid image.

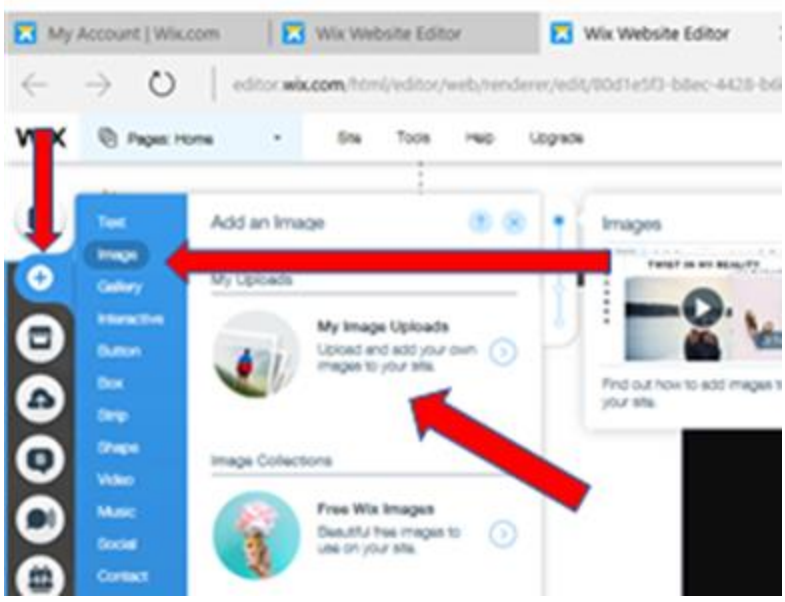

Figure 3.24: Shows the back page of the website and arrows pointing on the tabs that were clicked on to add lateral flow images.

- Save image by clicking on ‘’SAVE’’ on the top right icon.
- Return to the ‘’ADD’’ icon and go to “more”, then there will be HTML & Flash (emded a site option) which must be clicked on.
- Then a box prompting entry of website address appears. That is where a Google Analytics unique code should be pasted and saved to enable tracking of the website

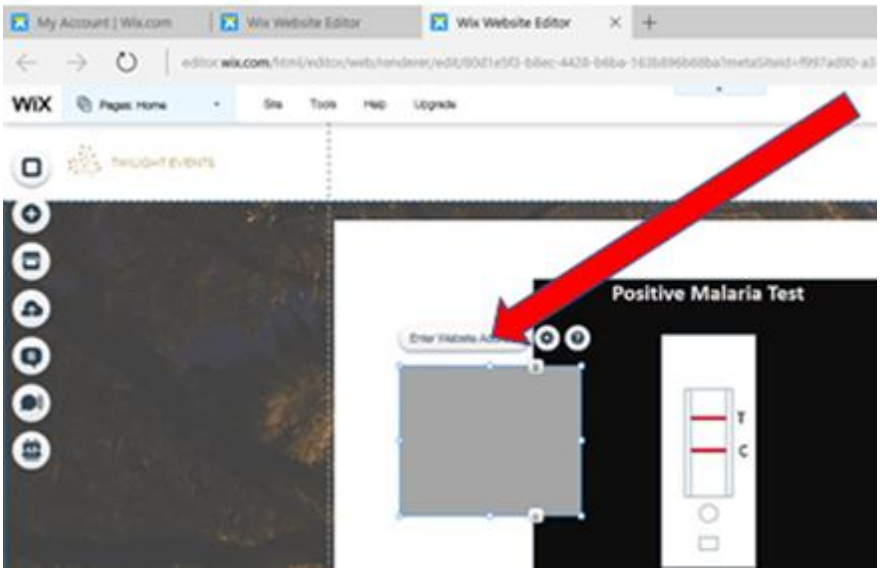

Figure 3.25: The picture shows a box at the back side of the website where a Google Analytics code is inserted and saved in order for users of the website to be recorded on Analytics. The red arrow pointed at the word “Enter website address”, where Google Analytics tracking codes are embedded.

- Go to “PUBLISH”, a message stating website has been published will appear, then go to ‘’DONE’’.

3.19 Settings on Google Analytics

Google Analytics (GA) is a support function in the form of a website that has a lot of features. The GA website was set to respond through capturing and monitoring of the personalized websites mentioned on Fig. 3.21 & 3.22. Linking the personalized websites with GA is a delicate process that enabled a lot of data to be available for this study. The process is described below:

- Login on Google Analytics and on the home page, go to ‘’ADMIN’’ as shown in Fig. 3.28.

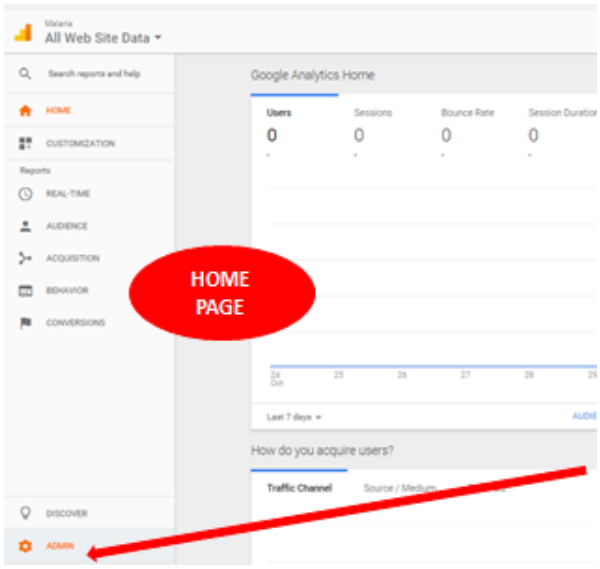

Figure 3.26: Shows the home page of Google Analytics and the arrow pointing at the “Admin” icon as part of a procedure leading to tracking codes.

- A page with ‘’Account’’, ‘’Property’’& ‘’View’’ appeared. On property, clicked on ‘’TRACKING INFO’’, and clicked on ‘’TRACKING CODE’’

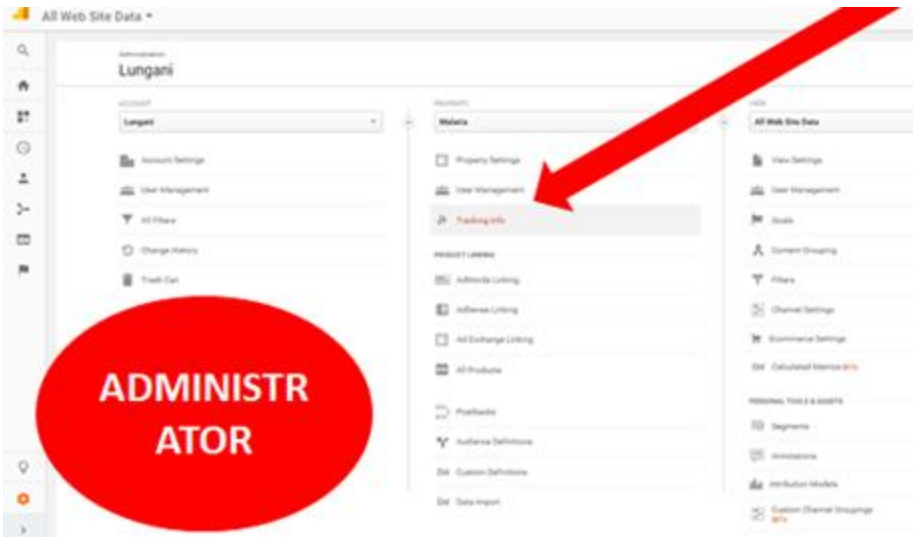

Figure 3.27: A page shows an arrow pointing at “Tracking info” on Google Analytics. The code copied and embedded on the website for statistics on website usage.

- A tracking code is displayed under website tracking, Global site. Copy all the codes in the rectangular box under ‘’Global Site Tag (gtag.js)’’
- Pasted the codes in the box mentioned in Fig. 3.25 and saved on wix.
- Once the above steps were completed, the website was liked with a unique QR code. By following the steps:
- On the Wix website “settings”, clicked on “MANAGE” on site address. The free domain of the website appeared.
- Copied the free domain and pasted it on the free QR code generator on website (URL). A QR code traceable to the website was be generated, then “DOWNLOADED” and “SAVED” it.

Figure 3.28: A picture shows an online quick response code generator. The arrow points where the website URL is inserted then the green button pressed to create a QR code.

After creating a website specific to either positive or negative, at the back of the website on settings and edit website, there is a unique link that was used to create a unique QR code. The link was copied and inserted on Fig. 3.28 and generated a QR code that wen scanned, links to a website.

.

Figure 3.29: Data generated over a 7 days period for scanned malaria diagnostic assays.

3.20 Google Analytics home

The data generated by users that scanned the QR codes over a 7 days period is shown on Fig. 3.29. The analysis shows that only two users (33% decreases from the usual number of users scanning) scanned the QR codes within the specified time period and they did a total of 6 sessions (100% of the whole scans done). The users scanning time period was 1 minute 31 seconds which is (13,625%) more time spent compare to usual time. 0% bounce rate was recorded during the scans and no user was currently on the site when the screenshot was taken (On Real Time Analysis). On the 11th of August, 2 users used the QR code test kit to test malaria as specified on the graph. No real time user active at the time of data collection.

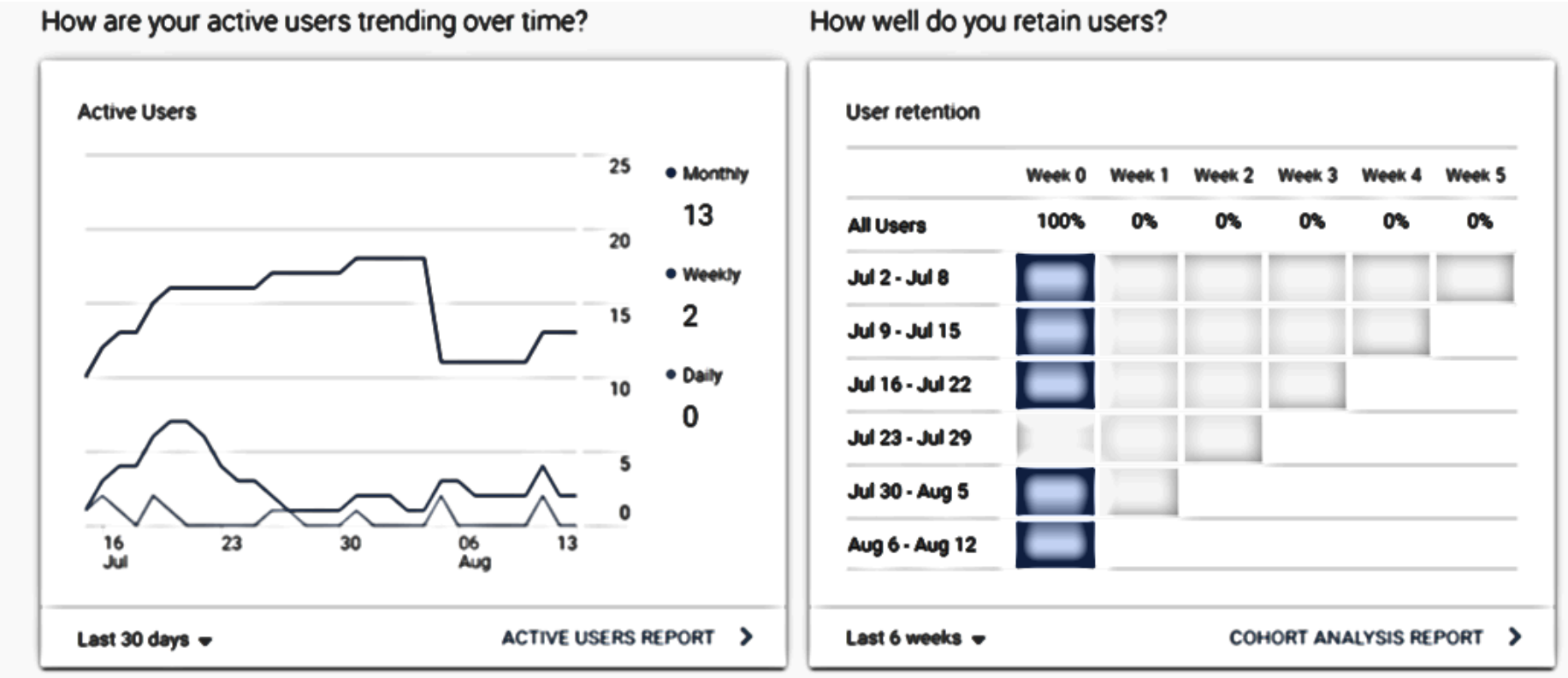

Figure 3.30: Data analysis of users of the scanned malaria diagnostic assays and frequency of users which shows numbers over a certain periods.

3.21 Active users trend over time

Data generated on Google Analytics on 1 month is expressed on Fig. 3.30**.** On a 30 days period the Analytics tracking of users that scanned the QR codes was graphically presented and a trend of usage was observed from 16 July to 13 August 2016. A rise in usage of the QR code embedded testing kit was observed on the 16th and 23rd of July in a 5 days range. A total of 13 users in 30 days was recorded, at least 2 users in a week and 0 users daily. The only frequency not picked up was a daily during the study.

3.22 Retention of users

Active users that use the testing kit through scanning of the QR barcode on a single day have their details captured and registered in the tracking system of Google Analytics. When the same user(s) scans on a deference date for the second time, the Analytics recognises the user as a returning and categorise them on retained users. A 100% was observed on all users as user retention from 2 – 8 July 2016, 9 – 15 July 2016, 16 – 22 July, 0% from 23 – 29 July, 100% from 30 July – 5 August and 100% from 6 – 12 August 2016. The users that scanned returned back to scan again and hence were classified as retained users.

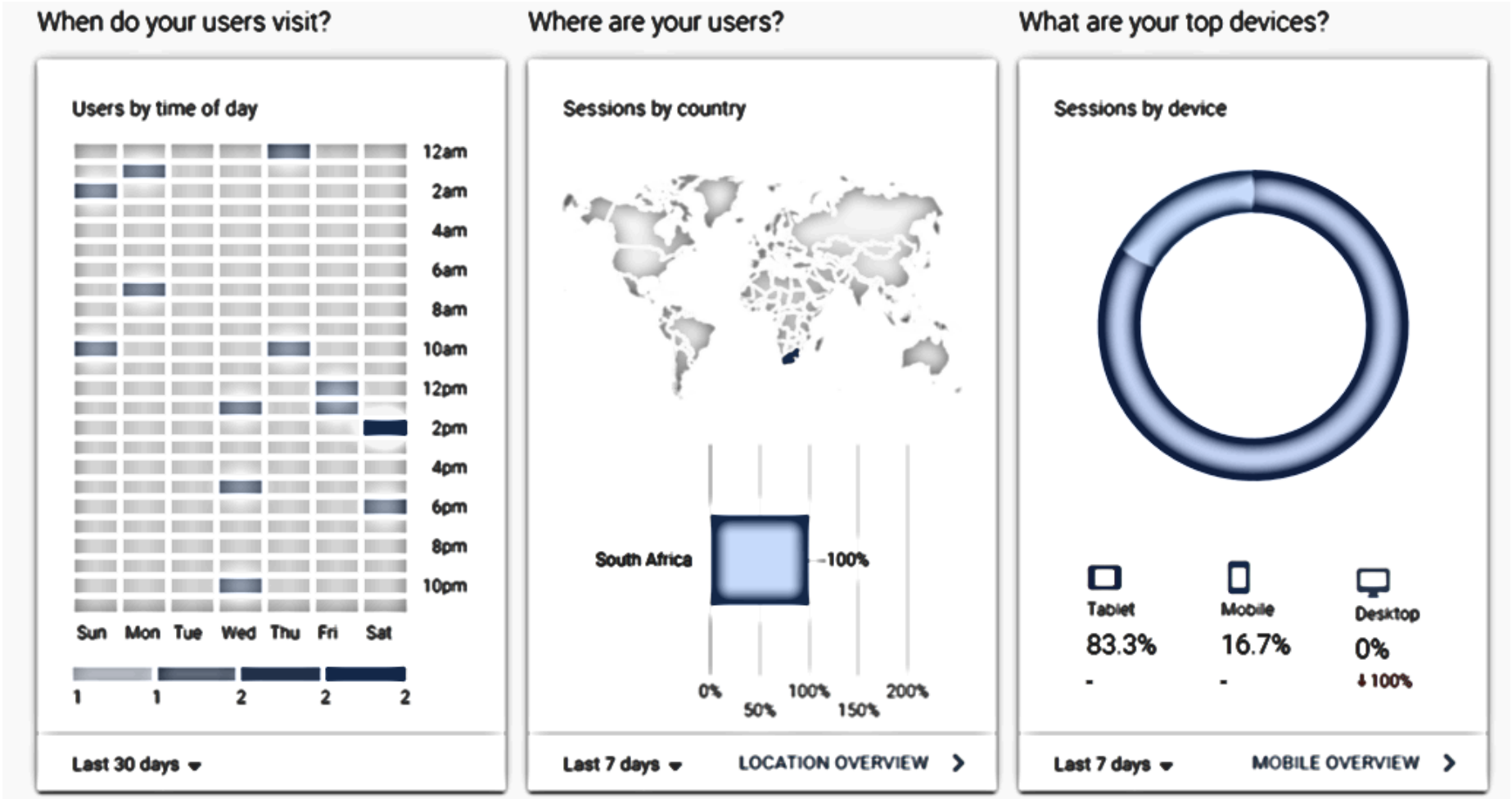

Figure 3.31: Geolocation of users and usage over a certain period as well the type of device that was used for each scanning.

3.23 Site visited times

This aspect of Google Analytics recorded the times in which the sites were visited, meaning when the scans of test kits were performed and made a statistical summary of the exact times and dates on a week when the scans were done. In Fig. 3.31, 2 users scanned on Friday, 1 at 2 am; one at 10 am, on Monday 2 users scanned; 1 at 1 am, one at 7 am, while on Tuesday no user scanned the test. On Wednesday, 3 users scanned test kits; 1 at 1 pm, 1 at 5pm and 1 at 10 pm. On Thursday only 2 users used the test and scanned, 1 at 12 am and 1 at 10 am. On Friday 2 users again, 1 at 12 pm and 1 at 1 pm. On Saturday two users scanned again at 2 pm and at 6 pm.

3.24 Location of users

The location overview shows the global position of users that scanned the QR codes. As seen in Fig. 3.31 on the centre image, most users were in South Africa hence RSA is the country from which the study originated.

3.25 Location of devices

Google Analytics is also able to pick up device types from which the link to website was accessed. On a 7 days period, 83.3% used a tablet to open our QR barcode links, 16.7% used a mobile phone and 0% on Desktop computer. This makes good sense as computers would rarely have QR code scanners hence no user could scan using a computer. The world map highlighting the location of all recorded Google Analytics scans for this research is posted on the Annexure and provides clear demographics while rendering GA a powerful tool in diagnostics. The Durban, Umbogintwini laboratory where the concept was discovered and experiments were conducted is shown under “Areas where studies were conducted”, the Randburg, Johannesburg laboratory where proof of concept was done is on the far right of the Annexure.

CHAPTER 4

Conclusion & Recommendations

4. Conclusion

A colloidal gold-labelled diagnostic kit for the rapid test of malaria parasite antigens (Plasmodium falciparum) was developed. The antibodies were successfully conjugated to the colloidal AuNPs. The test strip could be able to differentiate between positive and negative spiked samples for a recombinant pLDH antigen; this was shown by obtaining one line (control line) instead of two lines (control and test lines), but the appearance of the control line validated the test strip and also the colloidal gold-labelled antibodies. The kit was further demonstrated as a potential tool to be fabricated as a semi-quantitative lateral flow assay using an intensity reader. Through modification of the QR code, it is possible to collect data from the point-of-care through Google Analytics which offers statistical data through the website monitoring of participants scanning and real-time analytics results. Overall, this approach is best suited for tracking diseases using the testing kit and it links directly to the appropriate results of the test.

The studies using AuNPs were conducted successfully; UV–Visible is indeed a crucial technique when dealing with AuNPs since it helps on studying a wide variety of AuNPs properties. QR code system application to lateral flow was successfully achieved and the concept was proven to work across 9 countries as shown on Fig. 3.19. Google Analytics is a vital tool in the future of chemical and biological analyses and statistics of diseases in the country and internationally. The developed QR code lateral flow was successfully proved to work through several tests conducted in different cities in South Africa and internationally. The tracking of results using Google Analytics brought a great factor in the diagnostics research field. RGB codes have proven as a good tool for quantification of colored solutions where there are unknowns. The best R^2 value obtained from RGB color model was 0.9921 which is a good symbol for accuracy of the technique used. Monitoring of visitor statistics and activity of the website contributed immensely in this study which led to proving that status of results and specific location can be obtained using the developed test for malaria.

4.1 Recommendations

Further studies could examine simpler ways to use quick response technology in rapid testing kits. The developed testing kit uses two channel QR code overlaying mechanism that consists of negative and positive code determination. Further studies should expand to 3 channel codes overlaying where positive, negative and invalid are examined, and try different ways to use QR code in diagnosing malaria. Cell phone software should be developed to quantify antigen concentration after the testing is done and be able to report results of quantification through website and Google Analytics as done on this study.

4.2 References

Abraham, M., Massebo, F. and Lindtjørn, B. 2017. High entomological inoculation rate of malaria vectors in area of high coverage of interventions in southwest Ethiopia: Implication for residual malaria transmission. *Parasite Epidemiology and Control*, 2 (2): 61-69.

Agunloye, E., Gavriilidis, A. and Mazzei, L. 2017. A Mathematical Investigation of the Turkevich Organizer Theory in the Citrate Method for the Synthesis of Gold Nanoparticles. *Chemical Engineering Science*, 173: 275-286.

Ajmal, M. R., Abdelhameed, A. S., Alam, P. and Khan, R. H. 2016. Interaction of new kinase inhibitors cabozantinib and tofacitinib with human serum alpha-1 acid glycoprotein. A comprehensive spectroscopic and molecular Docking approach. *Spectrochimica Acta Part A: Molecular and Biomolecular Spectroscopy*, 159: 199-208.

Ajmal, M. R., Nusrat, S., Alam, P., Zaidi, N., Khan, M. V., Zaman, M., Shahein, Y. E., Mahmoud, M. H., Badr, G. and Khan, R. H. 2017. Interaction of anticancer drug clofarabine with human serum albumin and human α-1 acid glycoprotein. Spectroscopic and molecular docking approach. *Journal of Pharmaceutical and Biomedical Analysis*, 135: 106-115.

Amagliani, L., O'Regan, J., Kelly, A. L. and O'Mahony, J. A. 2017. Composition and protein profile analysis of rice protein ingredients. *Journal of Food Composition and Analysis*, 59: 18-26.

Ang, S. H., Thevarajah, T. M., Woi, P. M., Alias, Y. b. and Khor, S. M. 2016. A lateral flow immunosensor for direct, sensitive, and highly selective detection of hemoglobin A1c in whole blood. *Journal of Chromatography B*, 1015-1016: 157-165.

Aru, V., Lam, C., Khakimov, B., Hoefsloot, H. C. J., Zwanenburg, G., Lind, M. V., Schäfer, H., van Duynhoven, J., Jacobs, D. M., Smilde, A. K. and Engelsen, S. B. 2017. Quantification of Lipoprotein Profiles by Nuclear Magnetic Resonance Spectroscopy and Multivariate Data Analysis. *TrAC Trends in Analytical Chemistry*, 94: 210-219.

Atella, G. C., Bittencourt-Cunha, P. R., Nunes, R. D., Shahabuddin, M. and Silva-Neto, M. A. C. 2009. The major insect lipoprotein is a lipid source to mosquito stages of malaria parasite. *Acta Tropica*, 109 (2): 159-162.

Auburn, S. and Barry, A. E. 2017. Dissecting malaria biology and epidemiology using population genetics and genomics. *International Journal for Parasitology*, 47 (2–3): 77-85.

Ayyub, A., Saleem, M., Fatima, I., Tariq, A., Hashmi, N. and Musharraf, S. G. 2016. Glycosylated Alpha-1-acid glycoprotein 1 as a potential lung cancer serum biomarker. *The International Journal of Biochemistry & Cell Biology*, 70: 68-75.

Azikiwe, C. C. A., Ifezulike, C. C., Siminialayi, I. M., Amazu, L. U., Enye, J. C. and Nwakwunite, O. E. 2012. A comparative laboratory diagnosis of malaria: microscopy versus rapid diagnostic test kits. *Asian Pacific Journal of Tropical Biomedicine*, 2 (4): 307-310.

Babiker, H. A. and Walliker, D. 1997. Current views on the population structure of plasmodium falciparum: Implications for control. *Parasitology Today*, 13 (7): 262-267.

Bahadır, E. B. and Sezgintürk, M. K. 2016. Lateral flow assays: Principles, designs and labels. *TrAC Trends in Analytical Chemistry*, 82: 286-306.

Basco, L. K., Marquet, F., Makler, M. M. and Lebras, J. 1995. Plasmodium falciparum and Plasmodium vivax: Lactate-Dehydrogenase Activity and Its Application for in Vitro Drug Susceptibility Assay. *Experimental Parasitology*, 80 (2): 260-271.

Brossier, F., Sougakoff, W., Aubry, A., Bernard, C., Cambau, E., Jarlier, V., Mougari, F., Raskine, L., Robert, J. and Veziris, N. 2017. Molecular detection methods of resistance to antituberculosis drugs in Mycobacterium tuberculosis. *Médecine et Maladies Infectieuses*, 47 (5): 340-348.

Caperna, T. J., Shannon, A. E., Stoll, M., Blomberg, L. A. and Ramsay, T. G. 2015. Regulation of alpha-1 acid glycoprotein synthesis by porcine hepatocytes in monolayer culture. *Domestic Animal Endocrinology*, 52: 51-59.

Cheung, Y.-W., Dirkzwager, R. M., Wong, W.-C., Cardoso, J., D'Arc Neves Costa, J. and Tanner, J. A. 2017. Aptamer-mediated Plasmodium-specific diagnosis of malaria. *Biochimie*: 1-6.

Chistiakov, D. A., Melnichenko, A. A., Orekhov, A. N. and Bobryshev, Y. V. 2017. How do macrophages sense modified low-density lipoproteins? *International Journal of Cardiology*, 230: 232-240.

Choi, J.-S. and Meghani, N. 2016. Impact of surface modification in BSA nanoparticles for uptake in cancer cells. *Colloids and Surfaces B: Biointerfaces*, 145: 653-661.

Chow, B. W. and Gu, C. 2015. The Molecular Constituents of the Blood–Brain Barrier. *Trends in Neurosciences*, 38 (10): 598-608.

Cowman, A. F., Healer, J., Marapana, D. and Marsh, K. 2016. Malaria: Biology and Disease. *Cell*, 167 (3): 610-624.

Cruzat, A., Qazi, Y. and Hamrah, P. 2017. In Vivo Confocal Microscopy of Corneal Nerves in Health and Disease. *The Ocular Surface*, 15 (1): 15-47.

cvFitri, L. E., Iskandar, A., Sardjono, T. W., Erliana, U. D., Rahmawati, W., Candradikusuma, D., Saputra, U. B., Suhartono, E., Setiawan, B. and Sulistyaningsih, E. 2016. Plasma glutathione and oxidized glutathione level, glutathione/oxidized glutathione ratio, and albumin concentration in complicated and uncomplicated falciparum malaria. *Asian Pacific Journal of Tropical Biomedicine*, 6 (8): 646-650.

Dakić, Z., Ivović, V., Pavlović, M., Lavadinović, L., Marković, M. and Djurković-Djaković, O. 2014. Clinical significance of molecular methods in the diagnosis of imported malaria in returning travelers in Serbia. *International Journal of Infectious Diseases*, 29: 24-30.

Deagle, R. C., Wee, T.-L. and Brown, C. M. 2017. Reproducibility in light microscopy: Maintenance, standards and SOPs. *The International Journal of Biochemistry & Cell Biology*, 89: 120-124.

Del Pizzo, L., Foggia, P., Greco, A., Percannella, G. and Vento, M. 2016. Counting people by RGB or depth overhead cameras. *Pattern Recognition Letters*, 81 (Supplement C): 41-50.

Demir, S., Kaynak, R. and Demir, K. A. 2015. Usage Level and Future Intent of Use of Quick Response (QR) Codes for Mobile Marketing among College Students in Turkey. *Procedia - Social and Behavioral Sciences*, 181: 405-413.

Dormond, L., Jaton, K., de Vallière, S., Genton, B. and Greub, G. 2015. Malaria real-time PCR: correlation with clinical presentation. *New Microbes and New Infections*, 5: 10-12.

Endeshaw, T., Graves, P. M., Shargie, E. B., Gebre, T., Ayele, B., Yohannes, G., Zerihun, M., Genet, A., Melak, B., Kebede, A., Jima, D., Tadesse, Z., Ngondi, J., Mosher, A. W., Richards, F. O. and Emerson, P. M. 2010. Comparison of Parascreen Pan/Pf, Paracheck Pf and light microscopy for detection of malaria among febrile patients, Northwest Ethiopia. *Transactions of the Royal Society of Tropical Medicine and Hygiene*, 104 (7): 467-474.

Figueroa-Miranda, G., Feng, L., Shiu, S. C.-C., Dirkzwager, R. M., Cheung, Y.-W., Tanner, J. A., Schöning, M. J., Offenhäusser, A. and Mayer, D. 2018. Aptamer-based electrochemical biosensor for highly sensitive and selective malaria detection with adjustable dynamic response range and reusability. *Sensors and Actuators B: Chemical*, 255 (Part 1): 235-243.

Fischer, C., Wessels, H., Paschke-Kratzin, A. and Fischer, M. 2017. Aptamers: Universal capture units for lateral flow applications. *Analytical Biochemistry*, 522: 53-60.

Fu, X., Cheng, Z., Yu, J., Choo, P., Chen, L. and Choo, J. 2016. A SERS-based lateral flow assay biosensor for highly sensitive detection of HIV-1 DNA. *Biosensors and Bioelectronics*, 78: 530-537.

Gao, S. and Liu, J. 2017. Association between circulating oxidized low-density lipoprotein and atherosclerotic cardiovascular disease. *Chronic Diseases and Translational Medicine*, 3 (2): 89-94.

Garafutdinov, R. R., Galimova, A. A. and Sakhabutdinova, A. R. 2017. Polymerase chain reaction with nearby primers. *Analytical Biochemistry*, 518: 126-133.

Gordon, E. J., Shand, J. and Black, A. 2016. Google analytics of a pilot mass and social media campaign targeting Hispanics about living kidney donation. *Internet Interventions*, 6: 40-49.

Gulka, C. P., Swartz, J. D. and Wright, D. W. 2015. Ni(II)NTA AuNPs as a low-resource malarial diagnostic platform for the rapid colorimetric detection of Plasmodium falciparum Histidine-Rich Protein-2. *Talanta*, 135: 94-101.

Gunter, U. and Önder, I. 2016. Forecasting city arrivals with Google Analytics. *Annals of Tourism Research*, 61: 199-212.

Gupta, H., Srivastava, S., Chaudhari, S., Vasudevan, T. G., Hande, M. H., D'souza, S. C., Umakanth, S. and Satyamoorthy, K. 2016. New molecular detection methods of malaria parasites with multiple genes from genomes. *Acta Tropica*, 160: 15-22.

Hansen, F. K., Sumanadasa, S. D. M., Stenzel, K., Duffy, S., Meister, S., Marek, L., Schmetter, R., Kuna, K., Hamacher, A., Mordmüller, B., Kassack, M. U., Winzeler, E. A., Avery, V. M., Andrews, K. T. and Kurz, T. 2014. Discovery of HDAC inhibitors with potent activity against multiple malaria parasite life cycle stages. *European Journal of Medicinal Chemistry*, 82: 204-213.

Harani;, M. S., Beg;, M. A., Lubna Khaleeq, Adil;, S., Kakepoto;, G. N. and Khurshid, a. M. 2006. Role of ICT Malaria Immunochromatographic Test for Rapid diagnosis of Malaria. *Journal of Pakistan Medical Association*, 56 (4): 167-171.

Hathiwala, R., Mehta, P. R., Nataraj, G. and Hathiwala, S. 2017. LED fluorescence microscopy: Novel method for malaria diagnosis compared with routine methods. *Journal of Infection and Public Health*, 10 (6): 824-828.

Hayakawa, E. H. and Matsuoka, H. 2016. Detailed methodology for high resolution scanning electron microscopy (SEM) of murine malaria parasitized-erythrocytes. *Parasitology International*, 65 (5): 539-544.

Hayton, K., Dumoulin, P., Henschen, B., Liu, A., Papakrivos, J. and Wellems, T. E. 2013. Various PfRH5 polymorphisms can support Plasmodium falciparum invasion into the erythrocytes of owl monkeys and rats. *Molecular and Biochemical Parasitology*, 187 (2): 103-110.

Heinl, R. E., Tennant, H. M., Ricketts, J. C., Rice, C. R., Robinson, C. B., Sandesara, P. B., Moriarty, P. M. and Sperling, L. 2017. Lipoprotein-X disease in the setting of severe cholestatic hepatobiliary autoimmune disease. *Journal of Clinical Lipidology*, 11 (1): 282-286.

Henglin, Y., Dequan, L., Yaming, Y., Bo, F., Pinfang, Y., Xingliang, L., Chunfu, L., Ying, D. and Cangjiang, Y. 2003. Changes in susceptibility of Plasmodium falciparum to artesunate in vitro in Yunnan Province, China. *Transactions of the Royal Society of Tropical Medicine and Hygiene*, 97 (2): 226-228.

Hirayama, K., Takayama, K., Haruta, S., Ishibashi, H. and Takeuchi, I. 2017. Effect of low concentrations of Irgarol 1051 on RGB (R, red; G, green; B, blue)

colour values of the hard-coral Acropora tenuis. *Marine Pollution Bulletin*, 124 (2): 678-686.

Jain, P., Das, S., Chakma, B. and Goswami, P. 2016. Aptamer-graphene oxide for highly sensitive dual electrochemical detection of Plasmodium lactate dehydrogenase. *Analytical Biochemistry*, 514: 32-37.

Jamu, J. T., Lowi-Jones, H. and Mitchell, C. 2016. Just in time? Using QR codes for multi-professional learning in clinical practice. *Nurse Education in Practice*, 19: 107-112.

Julius, U. 2017. History of Lipidology and Lipoprotein Apheresis. *Atherosclerosis Supplements*,

Kavoshchian, M., Üzek, R., Uyanık, S. A., Şenel, S. and Denizli, A. 2015. HSA immobilized novel polymeric matrix as an alternative sorbent in hemoperfusion columns for bilirubin removal. *Reactive and Functional Polymers*, 96: 25-31.

Kim, Y. G. and Woo, E. 2016. Consumer acceptance of a quick response (QR) code for the food traceability system: Application of an extended technology acceptance model (TAM). *Food Research International*, 85: 266-272.

Kujda, M., Adamczyk, Z. and Ciesla, M. 2016. Monolayers of the HSA dimer on polymeric microparticles-electrokinetic characteristics. *Colloids and Surfaces B: Biointerfaces*, 148: 229-237.

Lal, S., McCart Reed, A. E., de Luca, X. M. and Simpson, P. T. 2017. Molecular Signatures in Breast Cancer. *Methods*, 131 (1): 135-146.

Ledesma, A. E., Chemes, D. M., Frías, M. d. l. A. and Guauque Torres, M. d. P. 2017. Spectroscopic characterization and docking studies of ZnO nanoparticle modified with BSA. *Applied Surface Science*, 412: 177-188.

Leopold, L. F., Tódor, I. S., Diaconeasa, Z., Rugină, D., Ştefancu, A., Leopold, N. and Coman, C. 2017. Assessment of PEG and BSA-PEG gold nanoparticles cellular interaction. *Colloids and Surfaces A: Physicochemical and Engineering Aspects*, 532 (5): 70-76.

Li, P., Xing, H., Zhao, Z., Yang, Z., Cao, Y., Li, W., Yan, G., Sattabongkot, J., Cui, L. and Fan, Q. 2015. Genetic diversity of Plasmodium falciparum histidine-rich protein 2 in the China–Myanmar border area. *Acta Tropica*, 152: 26-31.

Li, X., Fang, M., Zhang, J.-J. and Wu, J. 2017. Domain adaptation from RGB-D to RGB images. *Signal Processing*, 131 (Supplement C): 27-35.

Liu, Z.-L., Li, R., Zhang, X.-L., Qu, N. and Cai, L.-C. 2017. Direct anharmonic correction method by molecular dynamics. *Computer Physics Communications*, 213: 122-129.

Lorenzi, D., Vaidya, J., Chun, S., Shafiq, B. and Atluri, V. 2014. Enhancing the government service experience through QR codes on mobile platforms. *Government Information Quarterly*, 31 (1): 6-16.

Mak, W. C., Beni, V. and Turner, A. P. F. 2016. Lateral-flow technology: From visual to instrumental. *TrAC Trends in Analytical Chemistry*, 79: 297-305.

Mao, R., Ge, G., Wang, Z., Hao, R., Zhang, G., Yang, Z., Lin, B., Ma, Y., Liu, H. and Du, Y. 2018. A multiplex microfluidic loop-mediated isothermal amplification array for detection of malaria-related parasites and vectors. *Acta Tropica*, 178 (Supplement C): 86-92.

Markwalter, C. F., Davis, K. M. and Wright, D. W. 2016. Immunomagnetic capture and colorimetric detection of malarial biomarker Plasmodium falciparum lactate dehydrogenase. *Analytical Biochemistry*, 493: 30-34.

Martínez-Graña, A. M., Goy, J. L. and Cimarra, C. A. 2013. A virtual tour of geological heritage: Valourising geodiversity using Google Earth and QR code. *Computers & Geosciences*, 61: 83-93.

Mauriello, N., Pagnucci, G. S. and Winner, T. 1999. Reading between the code: the teaching of HTML and the displacement of writing instruction. *Computers and Composition*, 16 (3): 409-419.

Mdluli, P., Tetyana, P., Sosibo, N., van der Walt, H., Mlambo, M., Skepu, A. and Tshikhudo, R. 2014. Gold nanoparticle based Tuberculosis immunochromatographic assay: The quantitative ESE Quanti analysis of the intensity of test and control lines. *Biosensors and Bioelectronics*, 54: 1-6.

Mesken, J., Iltzsche, A., Mulac, D. and Langer, K. 2017. Modifying plasmid-loaded HSA-nanoparticles with cell penetrating peptides – Cellular uptake and enhanced gene delivery. *International Journal of Pharmaceutics*, 522 (1–2): 198-209.

Mesquita, T. C., Martin, T. G. O., Alves, E. R., Mello, M. B. C., Nery, A. F., Gomes, L. T. and Fontes, C. J. F. 2016. Changes in serum lipid profile in the acute and convalescent Plasmodium vivax malaria: A cohort study. *Acta Tropica*, 163: 1-6.

Mona, J., Kuo, C. J., Perevedentseva, E., Priezzhev, A. V. and Cheng, C. L. 2013. Adsorption of human blood plasma on nanodiamond and its influence on activated partial thromboplastin time. *Diamond and Related Materials*, 39: 73-77.

Moody, A. 2002. Rapid Diagnostic Tests for Malaria Parasites. *American Society for Microbiology*, 15: 66–78.

Moussa, E., Huang, H., Ahras, M., Lall, A., Thezenas, M. L., Fischer, R., Kessler, B. M., Pain, A., Billker, O. and Casals-Pascual, C. 2017. Proteomic profiling of the brain of mice with experimental cerebral malaria. *Journal of Proteomics*,

Muñoz-Bustos, C., Tirado-Guízar, A., Paraguay-Delgado, F. and Pina-Luis, G. 2017. Copper nanoclusters-coated BSA as a novel fluorescence sensor for sensitive and selective detection of mangiferin. *Sensors and Actuators B: Chemical*, 244: 922-927.

Nuovo, G., Paniccia, B., Mezache, L., Quiñónez, M., Williams, J., Vandiver, P., Fadda, P. and Amann, V. 2017. Diagnostic pathology of Alzheimer's disease from routine microscopy to immunohistochemistry and experimental correlations. *Annals of Diagnostic Pathology*, 28: 24-29.

Oduola, A. M. J., Omitowoju, G. O., Sowunmi, A., Makler, M. T., Falade, C. O., Kyle, D. E., Fehintola, F. A., Ogundahunsi, O. A. T., Piper, R. C., Schuster, B. G. and Milhous, W. K. 1997. Plasmodium falciparum:Evaluation of Lactate Dehydrogenase in Monitoring Therapeutic Responses to Standard Antimalarial Drugs in Nigeria. *Experimental Parasitology*, 87 (3): 283-289.

Oyeyemi, O. T., Sode, O. J., Adebayo, O. D. and Mensah-Agyei, G. O. 2016. Reliability of rapid diagnostic tests in diagnosing pregnancy and infant-associated malaria in Nigeria. *Journal of Infection and Public Health*, 9 (4): 471–477.

Padhi, S. S. and Pati, R. K. 2017. Quantifying potential tourist behavior in choice of destination using Google Trends. *Tourism Management Perspectives*, 24: 34-47.

Palisoul, M. L., Mullen, M. M., Feldman, R. and Thaker, P. H. 2017. Identification of molecular targets in vulvar cancers. *Gynecologic Oncology*, 146 (2): 305-313.

Philip, D. 2008. Synthesis and spectroscopic characterization of gold nanoparticles. *Spectrochimica Acta Part A: Molecular and Biomolecular Spectroscopy*, 71 (1): 80-85.

Piper, R., Lebras, J., Wentworth, L., Hunt-Cooke, A., Houze´ , S., Chiodini, P. and Makler, M. 1999. Immunocapture diagnostic assays for malaria using plasmodium lactate dehydrogenase (pLDH). *The American Society of Tropical Medicine and Hygiene*, 60 (1): 109–118.

Plaza, B. 2011. Google Analytics for measuring website performance. *Tourism Management*, 32 (3): 477-481.

Quesada-González, D. and Merkoçi, A. 2015. Nanoparticle-based lateral flow biosensors. *Biosensors and Bioelectronics*, 73: 47-63.

Ricks, K. M., Adams, N. M., Scherr, T. F., Haselton, F. R. and Wright, D. W. 2016. Direct transfer of HRPII-magnetic bead complexes to malaria rapid diagnostic tests significantly improves test sensitivity. *Malaria journal*, 15 (1): 399.

Rodrigues, M. M. and Soares, I. S. 2014. Gene-therapy for malaria prevention. *Trends in Parasitology*, 30 (11): 511-513.

Sarkar, D., Ghosh, I. and Datta, S. 2004. Biochemical characterization of Plasmodium falciparum hypoxanthine-guanine-xanthine phosphorybosyltransferase: role of histidine residue in substrate selectivity. *Molecular and Biochemical Parasitology*, 137 (2): 267-276.

Scherr, T. F., Gupta, S., Wright, D. W. and Haselton, F. R. 2016. Mobile phone imaging and cloud-based analysis for standardized malaria detection and reporting. *Scientific reports*, 6: 28645.

Scherr, T. F., Gupta, S., Wright, D. W. and Haselton, F. R. 2017. An embedded barcode for “connected” malaria rapid diagnostic tests. *Lab on a Chip*, 17 (7): 1314-1322.

Singla, R., Soni, S., Padwad, Y. S., Acharya, A. and Yadav, S. K. 2017. Sustained delivery of BSA/HSA from biocompatible plant cellulose nanocrystals for in vitro cholesterol release from endothelial cells. *International Journal of Biological Macromolecules*, 104, Part A: 748-757.

Tahoun, S. S., Deaf, A. S., Gentzis, T. and Carvajal-Ortiz, H. 2017. Modified RGB-based kerogen maturation index (KMI): Correlation and calibration with classical thermal maturity indices. *International Journal of Coal Geology*: 1-14.

Thaxton, C. S., Rink, J. S., Naha, P. C. and Cormode, D. P. 2016. Lipoproteins and lipoprotein mimetics for imaging and drug delivery. *Advanced Drug Delivery Reviews*, 106: 116-131.

Tiwari, S., Garnier, G. and Rao, V. R. 2017. One dimensional zinc oxide nanostructures assisted paper-based blood-plasma separation. *Vacuum*, 146: 586-591.

Turkevich, J., Stevenson, P. C. and Hillier, J. 1951. A study of the nucleation and growth processes in the synthesis of colloidal gold. *Discussions of the Faraday Society*, 11 (0): 55-75.

Vieira, J. L. F., Borges, L. M. G., Ferreira, M. V. D., Rivera, J. G. B. and Gomes, M. d. S. M. 2016. Patient age does not affect mefloquine concentrations in erythrocytes and plasma during the acute phase of falciparum malaria. *The Brazilian Journal of Infectious Diseases*, 20 (5): 482-486.

Wang, J., Guo, Y., Liu, B., Cheng, C., Wang, Z., Han, G., Gao, J. and Zhang, X. 2011. Spectroscopic analyses on interaction of bovine serum albumin (BSA) with toluidine blue (TB) and its sonodynamic damage under ultrasonic irradiation. *Journal of Luminescence*, 131 (2): 231-237.

Wang, Q., Rizk, S., Bernard, C., Lai, M. P., Kam, D., Storch, J. and Stark, R. E. 2017. Protocols and pitfalls in obtaining fatty acid-binding proteins for biophysical studies of ligand-protein and protein-protein interactions. *Biochemistry and Biophysics Reports*, 10: 318-324.

Wang, Z.-p., Zhang, S., Liu, H.-z. and Qin, Y. 2014. Single-intensity-recording optical encryption technique based on phase retrieval algorithm and QR code. *Optics Communications*, 332: 36-41.

Wong, J. X., Li, X., Liu, F. S. and Yu, H.-Z. 2015. Direct Reading of Bona Fide Barcode Assays for Diagnostics with Smartphone Apps. *Scientific reports*, 5: srep11727.

Yegneswaran, B., Alcid, D. and Mohan, J. 2009. Plasmodium knowlesi: An Important Yet Overlooked Human Malaria Parasite. *Mayo Clinic Proceedings*, 84 (7): 664.

Zhang, D. Z. and Dhakal, T. R. 2017. Shock waves simulated using the dual domain material point method combined with molecular dynamics. *Journal of Computational Physics*, 334: 240-254.

Zhang, L., Yu, L., Zhang-Van Enk, J., Huang, G. and Zhang, J. 2017. Phase Behavior of a Fc-fusion Protein Reveals Generic Patterns of Ion-specific Perturbation on Protein-Protein Interactions. *Journal of Pharmaceutical Sciences*, 106 (11): 3287–3292.

Zhang, Y.-h., Tang, L., Liu, X.-j., Liu, L.-l., Cao, W.-x. and Zhu, Y. 2014. Modeling Dynamics of Leaf Color Based on RGB Value in Rice. *Journal of Integrative Agriculture*, 13 (4): 749-759.

Zhao, S., Li, Z., Li, Y., Yu, J., Liu, G., Liu, R. and Yue, Z. 2017. BSA-AuNCs based enhanced photoelectrochemical biosensors and its potential use in multichannel detections. *Journal of Photochemistry and Photobiology A: Chemistry*, 342: 15-24.

ANNEXURES

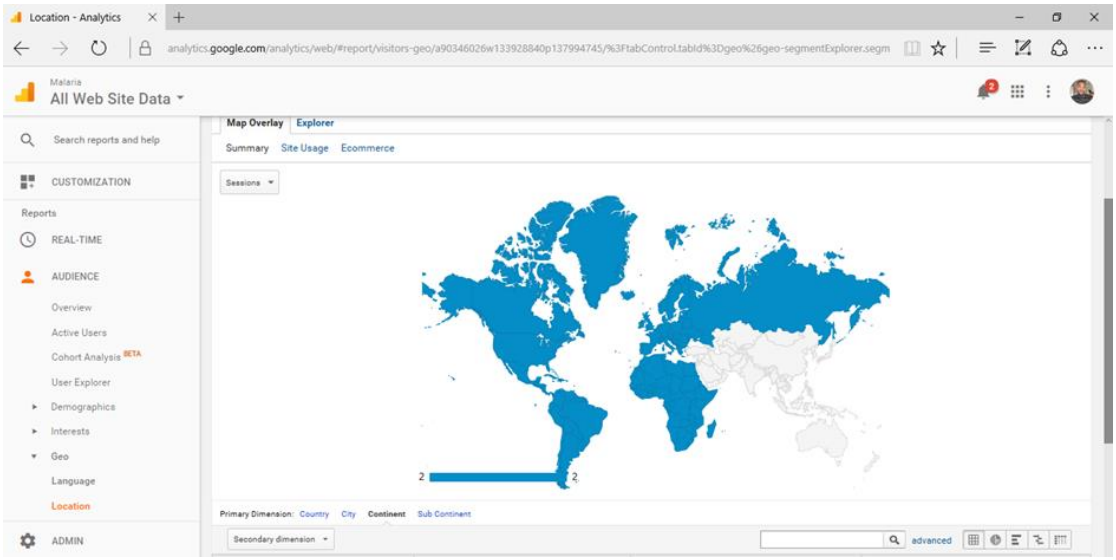

Annexure 1: Map highlighting locations of GA Scans recorded

Annexure 2: Arial view of the areas where studies were conducted

PUBLICATION